FLUORESCENCE RECOVERY AFTER PHOTOBLEACHING MEASUREMENTS OF SOLUTE DIFFUSION THROUGH HYDROGELS

by

Nicholas Angel Hadjiev

A thesis submitted to the Department of Chemical Engineering

In conformity with the requirements for

the degree of Master of Applied Science

Queen's University

Kingston, Ontario, Canada

October, 2014

Abstract

The distribution of therapeutic agents such as proteins or drug-loaded nanoparticles within a hydrogel following release influences their rate of absorption at the desired site of action. For formulation design purposes, it is, therefore, important to be able to predict their diffusivity within vehicles like the hydrogel. For this purpose, the diffusivity of solute probes within a hydrogel can be estimated using a mathematical expression based on describing the diffusion of spheres within a macromolecular matrix.

The assumptions of the obstruction-scaling model were assessed using fluorescence recovery after photobleaching. The obstruction model demonstrated excellent predictive capabilities for solute diffusion in polymer solutions using different molecular agents as shown through the work of Zhang and Amsden. To extend its applicability to hydrogels, the assumption must be valid that the correlation length of a hydrogel is the same as that of a polymer solution at equivalent concentrations. The results in this study confirm the validity of this assumption by comparing the predictions of the obstruction model to diffusion measurements of FITC-dextran (4, 10, 20, 40 kDa) in alginate-methacrylate gels. The model provided good predictions for small diffusing agents (4, 10 kDa) and underestimated the diffusion coefficients of dextrans exceeding 20 kDa. This difference was attributed to reptation effects that become more influential as the solute radius approaches the correlation length of a network.

Acknowledgements

I would like to express the deepest appreciation to my supervisor, Dr. Brian Amsden, for providing the research guidance throughout my Master's in chemical engineering here at Queen's University. He has given me an opportunity to work on a unique project that was certainly an enjoyable experience. Dr. Amsden has instilled in me the confidence to pursue my dreams and, for this, I can never repay him. I wish him good health, happiness, and extend my wishes to his family.

In addition, my thanks to Fei Chen and Jian Yang for their guidance on the NMR portion of this thesis. They are both very talented researchers and I wish them the best in life. My gratitude goes to the Amsden lab: Dale Marecak, Julian Chesterman, Moira Vyner, Ginger Chen, and Sara Mohajeri. It has been a memorable experience.

This thesis would not have been possible without the love and support of my family and partner. Thank you for everything that you have done for me. I owe a great debt for your kindness and guidance.

Table of Contents

List of Figures

List of Tables

List of Abbreviations

AEMA	2-aminoethyl methacrylate
ALG	Alginate
BSA	Bovine serum albumin
CSLM	Confocal scanning laser microscope
DLS	Dynamic light scattering
DOSY	Diffusion-ordered spectroscopy
EDC	N-(3-dimethylaminopropyl)-N’-ethylcarbodiimide
EDTA	Ethylenediaminetetraacetic acid
FCS	Fluorescence correlation spectroscopy
FDX	FITC-dextran
FITC	Fluorescein isothiocyanate
FRAP	Fluorescence recovery after photobleaching
GDM	Generalized disk model
HV	High voltage
I2959	2-hydroxy-1-[4-(2-hydroxyethoxy)phenyl]-2-methyl-1-propanone
MALG	Methacrylated alginate
MEHQ	Hydroquinone monomethyl ether
MES	2-morpholinoethanesulfonic acid
MWCO	Molecular weight cutoff
NHS	N-hydroxysuccinimide
NMR	Nuclear magnetic resonance
PA	Poly(2-propenamide)
PDMS	Poly(dimethyl siloxane)

PEG	Poly(ethylene glycol)
PEMA	Poly(ethyl methacrylate)
PFG	Pulse-field-gradient
PMMA	Poly(methyl methacrylate)
PSF	Point spread function
PVA	Poly(vinyl alcohol)
PVME	Poly(vinyl methyl ether)
ROI	Region of interest
RPM	Rotations per minute
S/N	Signal to noise ratio
SLS	Static light scattering
UDM	Uniform disk model
UV	Ultra violet

Chapter 1

Introduction

1.1 Preamble

Diffusion is fundamental to the migration of agents such as nutrients, signaling molecules, and drugs in the body. In recent years, extensive efforts have been devoted to the development of site-specific drug delivery systems to prolong, localize, and treat diseased tissue. Among numerous systems, which have been employed as vehicles or rate-controlling barriers, the hydrogel has gained considerable interest for its unique properties, such as its high water content and mechanical properties similar to those of many soft tissues. For this reason, the hydrogel is considered to be an excellent vehicle in drug delivery. The delivery of a drug prior to release from a transport vehicle like the hydrogel may directly influence its rate of absorption at the expected site of delivery. For formulation design purposes, it is, therefore, useful to be able to predict the diffusion coefficient of solute in hydrogels.

Several mathematical expressions have been proposed over the past few decades to provide *a priori* predictions of solute diffusion in hydrogels. Very few models have been able to provide a consistent explanation of the transport phenomena. This lack of a descriptive relationship between the observed and the predicted limits the potential utility of these systems until such a relation is derived. For this reason, it is important to understand the factors that govern solute diffusion in hydrogels and recognize the means by which such factors influence the phenomenon. Mathematical relationships will be reviewed in the following sections based on different diffusion concepts that describe the movement of solute in polymer solutions and gels. It would be constructive to review the general properties of the hydrogel prior to introducing these concepts.

1.2 General Properties of hydrogels

Hydrogels are macromolecular networks that may embody any polymer that enables the system to absorb at least 10-20% of its own weight in water while maintaining its original three-dimensional shape.[1] They consist of water soluble polymer chains that have been cross-linked either chemically or cohesively through covalent bonds, hydrogen bonds, van der Waals forces, ionic bonds, or physical entanglments.[2] The hydrogel may be formulated in a variety of shapes and sizes, including but not limited to, slabs, spheres, microparticles, nanoparticles, and thin films.[3]

The properties of the hydrogel are defined by the nature of the polymer that constitutes its framework. Its capability to absorb water mostly arises from any hydrophilic moieties attached to its network, whereas its resistance to swelling is governed by the extent of its cross-link density. The properties of the solvent may also have a profound effect on the hydrogel by influencing the degree and rate of swelling that the gel may experience.[4]

Hydrogels are readily used in drug delivery because of their unique bulk and surface properties.[5,6] They may demonstrate varying degrees of hydrophilicity, permeability, elasticity, mechanical strength, and transparency.[7] Their well tolerated tissue response is often promoted by high water content, mechanical similarities and, in some instances, compositional similarities to the extracellular matrix in the human body.[8]

The macromolecular network of the hydrogel defines its formative and mechanical properties but also obstructs diffusion, often by rejecting the movement of solute under circumstances in which the size of the diffusant exceeds the average end-to-end distance between the polymer chains in a network, otherwise referred to as the correlation length (Figure 1).[9,10] Diffusants with hydrodynamic radii that approach the correlation length of a gel may experience obstruction effects that negate their mobility.[11] This becomes a crucial factor in applications that rely on diffusion as a mechanism of transport such as controlled drug delivery.

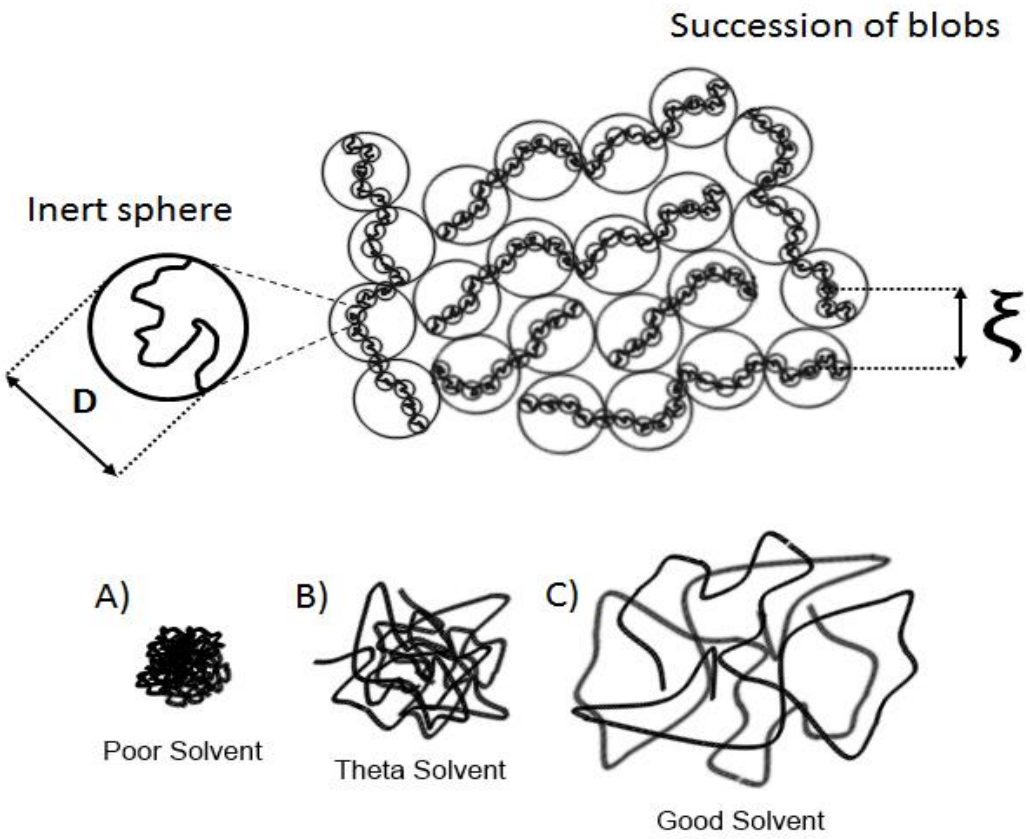

Figure 1: Correlation length of a polymer network*

A concept image shows a semi-dilute solution with stochastic polymer chains that are divided into a series of inert nanospheres of size D, an idea initially proposed by H. Benoit.[12] *The nanospheres are encased in a succession of blobs. Each blob is defined by a highly extended chain in the absence of electrolyte screening. Inside one blob, the polymer chain does not interact with nearby chains by reason of excluded volume. The same argument can be applied to the spheres. On scales that are smaller than the distance between neighboring chains, such as D, there are mostly monomers and solvent molecules, with little to no information on the general distance between nearby chains, i.e. nanospheres. However, on scales that are larger than the distance between neighboring chains, greater than ξ, there are many other chains, and the resulting network may then be defined as a succession of blobs that conform to a random walk.*[12] *The diameter of the blobs is defined as the correlation length (ξ) and by extension represents the average distance between the chains in a polymer network.*[12] *Neutral chains in poor solvents will collapse (A), in theta solvents will be a random walk (B), and in good solvents will be random and self-avoiding (C).*

**Figure 1 was developed based on a conceptual drawing by Dou and Colby.*[13]

1.3 Hydrogel Applications

Hydrogels have been employed as materials for tissue engineering scaffolds in regenerative medicine, as materials to control the release of therapeutic drugs, in separation processes such as gel electrophoresis,

and in biosensors.[14–19] The extent of their exclusive and often tunable properties assures the material a degree of multifold applicability; however, it is frequently the structure and functional properties of the gel that govern its propriety for specific applications. For example, stimuli-responsive hydrogels have the ability to swell or constrict in response to environmental stimulation. The three most common factors that may elicit such a response are variations in temperature, ionic strength, and pH.[20] Responsive systems have gained tremendous interest in drug delivery disciplines, often designed in principle for the delivery of sensitive proteins like insulin.[21–23]

Hydrogels are suitable for applications that have direct/prolonged contact with tissues such as burn wound dressings, implants, scaffolds, and contact lenses.[24] The contact lens, for example, relies on the physiochemical properties of a material to deliver an effective and potentially comfortable alternative to wearing glasses. The success of the lens is directly related to its derived structure-property relationship with a strong dependency on the following key properties: oxygen permeability, hydration, optical clarity, degree of comfort, and mechanical integrity.[25] Traditional rigid contacts were deficient in delivering several of these properties and have consequently been replaced by silicone hydrogels.[26]

A remarkable amount of research into hydrogels has arisen due to their widespread use in pharmaceutical, agricultural, biomedical, and consumer-oriented industries.[27] The hydrogel is generally affiliated with drug delivery because its porosity easily permits the loading of a drug or macroscopic body under biological conditions.[28] There are several factors to consider that may influence the delivery and uptake of a drug when formulating the design of hydrogels for drug delivery applications. For example, the release rate of a drug from a gel may directly affect its rate of absorption at the site of action; as such, it is important to have knowledge on its diffusion coefficient within the gel prior to release.

1.4 Mutual diffusion and self-diffusion coefficients

Chemical potential gradients within a solution, free from convection currents, will produce a spontaneous flow of matter that tends to reduce those differences. In binary systems, such as a solution

comprised of a solvent and a single electrolyte, the diffusion is described by a diffusion coefficient according to Fick's first law,[29,30]

$$J = -\frac{D c_i}{RT}\frac{\partial \mu_i}{\partial x} \quad [1]$$

where, J is the diffusion flux, D is the diffusion coefficient, c is the concentration, x is the distance, R is the universal gas constant, T is the absolute temperature, and μ is the chemical potential. The diffusion coefficient in Equation 1 corresponds to the solvent and the solute, as both entities are mutually involved in the diffusion process. The flow of the solute must be met with a counter flow of the solvent that is governed by a chemical potential gradient in opposite direction for the two species.[29] This phenomenon is referred to as mutual diffusion and is described by a mutual diffusion coefficient. Mutual diffusion coefficients can be expressed in respect to their intrinsic diffusion coefficients by the following relationship,[31]

$$D_m = V_A C_A (D_B - D_A) + D_A \quad [2]$$

where, D_m is the mutual diffusion coefficient, A & B are the respective components in the system, generally A is the solute and B the solvent, C_A is the concentration of species A, V_A is the constant volume of species A, and D_i is the intrinsic diffusion coefficient of either component. In systems that are already equilibrated in the absence of a chemical potential gradient, there is no net mass transfer, but the species are still in constant motion. This phenomenon is referred to as Brownian motion and is described by a self-diffusion coefficient, otherwise referred to as a spontaneous diffusion coefficient.[32] Spontaneous diffusion results from molecular collisions driven by the thermal energy of the entities within the boundaries of a system and results in a net displacement of zero for the individual components. In circumstances when the concentration of the solute is very low, the diffusion becomes tracer diffusion and is described by a tracer diffusion coefficient.[32] Spontaneous diffusion coefficients can be related to their intrinsic coefficients using the following expression,[33]

$$D_A = D_s C_A \left(\frac{\partial \mu_A}{\partial C_A}\right) \quad [3]$$

where, D_s is the spontaneous diffusion coefficient, and μ is the chemical potential of the species. Diffusion coefficients, whether mutual or spontaneous, have been studied for decades using a variety of techniques, such as gravimetry, membrane penetration, fluorescence, nuclear magnetic resonance (NMR), dynamic light scattering (DLS), and static light scattering (SLS).[32]

1.5 Solute diffusion in hydrogels

Diffusion is responsible for the movement of matter from one part of a system to another, often arising from random molecular motions. In gases and liquids, diffusion can be described by theories and successfully predicted with models that are reliant on factors such as temperature, solute size, viscosity, and pressure.[32] Diffusion in hydrogels is slightly more complex, requiring attention to additional parameters, such as polymer chain radius, polymer swelling, polymer chain flexibility, electrostatic interactions between polymer chains, correlation length, solvent interactions, and so on. As a result, it becomes a real challenge to model the diffusion of small and large molecules in gels.[32]

In hydrogels, the transport of a probe fundamentally depends on its ability to find an opening large enough to allow passage through the mesh-like matrix of chains that define the system. Molecular probes that are unable to accomplish this are generally bound to remain encapsulated within the hydrogel.[2] Over the past few decades, several arguments have been proposed to describe solute diffusion in hydrogels in an effort to bridge the divergence between the observed the predicted, resulting in three unique diffusion theories: hydrodynamic, free volume, and obstruction theory.[32]

1.6 Hydrodynamic theory

In hydrodynamic theory, the hydrodynamic friction between the polymer chains, the solvent, and the diffusing agent are taken into consideration. These interactions can be broken down into three concepts: (1) the friction between the polymer chains and the probe, probably the most influential; (2) the friction

between the probe and the solvent; and (3) the friction between the polymer chains and the solvent.[32] The first hydrodynamic model was introduced by Cukier in 1984 in a publication that studied the diffusion of Brownian spheres in semi-dilute polymer solutions.[34] Other notable hydrodynamic models were developed by Altenberger and Phillies.[35,36]

1.7 Free volume theory

In free volume theory, the movement of a solute from one part of a system to another is accomplished by occupying voids between the solvent molecules at any given point in time. Free volume can be defined as the volume of a system at a given temperature minus the volume of that same system at 0 K.[32] Diffusion in free volume theory is described as the movement of an agent between the transient pockets created by the random distribution of free volume in a system that occupies space by all the species present within its boundaries.[32] Free volume concepts are well-known in science and rely on the assumption that voids are aptly enabling the diffusion of solute in polymer solutions. The first free volume diffusion model was introduced by Fujita in 1961.[37] Other notable models were derived by Yasuda *et al.* and Vrentas and Duda.[38,39]

1.8 Obstruction theory

In obstruction theory, the polymer chains within a solution or hydrogel are assumed to be static, at least with respect to the movement of the solute. The velocity magnitude of the diffusant exceeds the mobility of an individual polymer chain within a network to such a degree that the transient matrix appears immobile from the perspective of the probe.[11] The network is, therefore, treated as a complex impenetrable system that deflects the movement of solute. The presence of these chains increases the mean path length of molecular agents and forces them to find physical openings within the matrix if they are to diffuse. The obstruction concept was first introduced by Fricke in 1924 in a publication that studied the electric conductivity of spheroids dispersed in dog blood.[40] Other notable models were derived by Ogston *et al.* and Mackie and Meares.[41,42] Recently, Amsden derived an obstruction model to describe the

diffusion of solute in polymer solutions and hydrogels. The obstruction-scaling model, as it was coined, demonstrated excellent predictive capabilities for tracer diffusion in alginate solutions in a study by Zhang and Amsden.[2] In this thesis, the obstruction-scaling model was compared to experimental measurements of solute diffusion in hydrogels to investigate the validity of its assumptions and whether its predictions are dependable for hydrogels.

1.9 Conceptual limitations

There is no general expression or conceptual argument that is consistent in describing the movement of solute in hydrogels or polymer solutions because the observed diffusion process is complex. Each theory has its merits and limitations. Free volume theory was at one point in time the most invoked, often applied to situations for which the selected model and its derived assumptions were inappropriate.[2] For this reason, free volume models are now rarely used.

Obstruction theory was derived to take into consideration the deflection of solute by polymer chains, forcing detours throughout a network and an increase in the mean path length of the diffusing agent. They were conceptually appealing and apt to define properties such as chain flexibility and solute radius. Obstruction models were among the first models, but they were underachieving at high volume fractions of polymer when the hydrodynamic friction between the chains and the solute was no longer negligible. Hydrodynamic concepts were developed to compensate for the absence of hydrodynamic drag in obstruction theory in an attempt to describe solute diffusion in these highly concentrated systems.[32] These theories and their respective models should be applied with care for analysis and always within their derived assumptions to be of any use.[32]

1.10 Obstruction-scaling diffusion model: history

The obstruction-scaling model was first introduced in 1998 in a publication that studied the mechanisms and models for solute diffusion within hydrogels, where it was compared to notable expressions derived by others using the literature data available at the time.[2] The model was then applied

to polymer solutions in 2002, using a similar approach, by assuming that the polymer chains within a solution are relatively static in the semi-dilute regime.[43] In its original publication, the model utilized scaling concepts proposed by de Gennes and extended by Schaefer to describe the correlation length of a polymer network in relation to the thermodynamic properties of its chains.[12,44] Schaefer reasoned that the correlation length can be modeled using the following relationships in accordance with the correct polymer-solvent regime (Table 1),[44]

Table 1: Schaefer's scaling methods

Good	$\xi \sim a\Phi^{-0.75}\, {C_\infty}^{-0.25}(1-2\chi)^{-0.25} \sim \kappa\Phi^{-0.75}$	[4]
Marginal	$\xi \sim \frac{{C_\infty}^{1.5} a}{(1-2\chi)^{0.5}}\Phi^{-0.5} \sim \kappa\Phi^{-0.5}$	[5]
Theta	$\xi \sim \frac{a{C_\infty}^{2}}{(wa^{-6})^{0.5}}\Phi^{-1} \sim \kappa\Phi^{-1}$	[6]

where, ξ is the correlation length, C_∞ is the characteristic ratio of the polymer, χ is the Flory Huggins interaction parameter, Φ is the polymer volume fraction of the polymer, w is the excluded volume, κ is a grouped parameter, and a is the equivalent bond length of the monomer. The initial relationship proposed by de Gennes articulates that the correlation length can be inferred from a simple scaling argument in all polymer solutions,[12]

$$\xi = R_g \left(\frac{c}{c^*}\right)^{\nu} \quad [7]$$

where, R_g is the radius of gyration (Figure 2), c* is the polymer overlap concentration (Figure 3), c is the polymer concentration, and ν is a scaling parameter, for which a θ-solvent $\nu = 1$, good solvent $\nu = 0.75$, and marginal solvent $\nu = 0.5$. Equation 7 was assumed to be applicable as a general expression to describe

the average distance between the polymer chains within a solution. Zhang and Amsden used these scaling concepts to determine whether the obstruction model could provide *a priori* predictions of the tracer diffusion coefficient of globular proteins in sodium alginate solutions in 2006.[11] The results showed that the obstruction model was able to provide accurate predictions of the diffusion coefficient for polymer solutions, suggesting, on one hand, that the correlation length of a semi-dilute polymer solution can be described by Equation 7 within the limitations of the obstruction-scaling model; and the other, that spontaneous diffusion in semi-dilute polymer solutions is likely governed by obstruction theory. To extend the model's applicability to hydrogels, the assumption must be valid that the correlation length of a polymer network in the solution state is the same as that in the gel state at equivalent concentrations. The validity of this assumption will be addressed in the sections that follow.

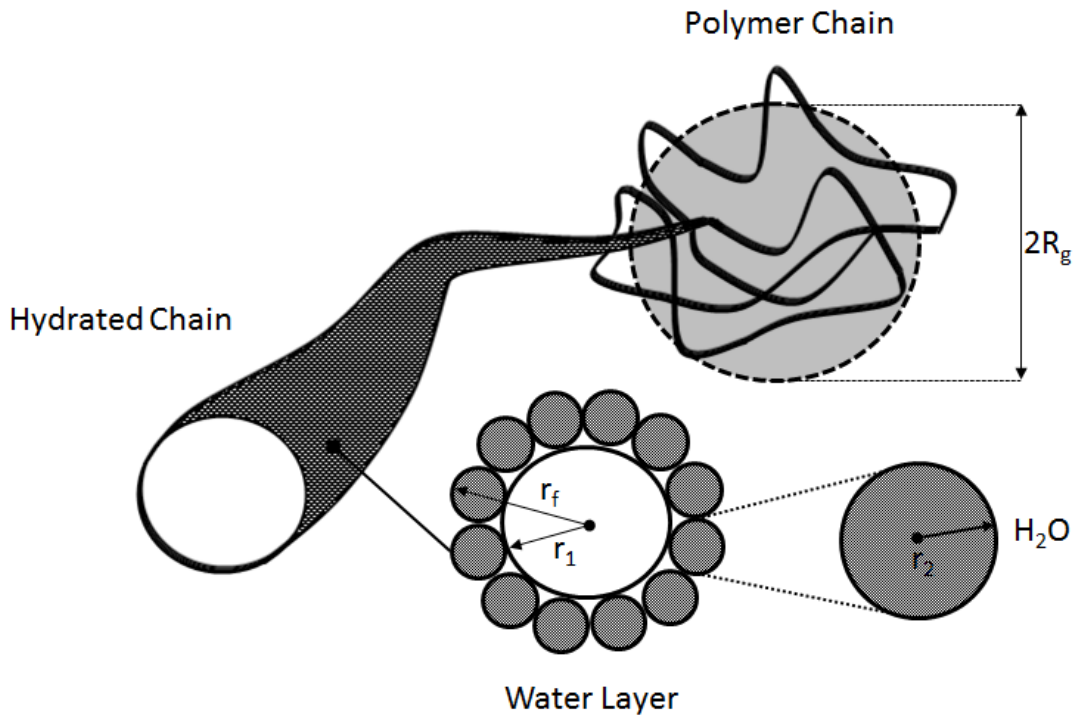

Figure 2: Radius of polymer/gyration

A concept image of a polymer chain is portrayed as an individual coil that is isolated from other chains. The cross-sectional radius of the bare chain is extended by a thin layer of water as a result of its hydration in solution. If r_2 is the radius of a water molecule and r_1 is the radius of the bare chain, then the hydrated cross-sectional radius (r_f) is equal to $r_1 + 2r_2$. The radius of gyration (R_g) describes the average size of the polymer chain relative to its center of mass.

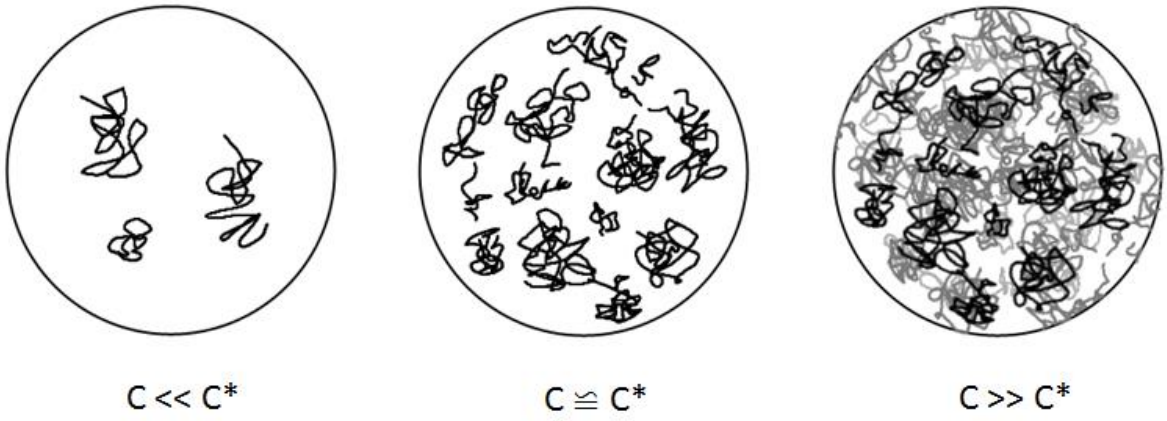

Figure 3: Overlap concentration*

The overlap concentration describes the critical point in a polymer solution when the polymer chains are at the brink of overlap. Below c, the polymer chains are dispersed and rarely interact as it is unlikely that they will encounter one another. However, as c approaches c*, the chains develop a sense of other chains. Above c*, the polymer chains overlap and become entangled forming a network.*

*Figure 3 was developed based on a conceptual drawing from Teraoka Iwao.[45]

1.11 Obstruction-scaling diffusion model: derivation

The obstruction-scaling model has been derived elsewhere.[10] However, it would be constructive to summarize its derivation for clarity. The model is based on the premise that solute diffusion is driven by the ability for a molecular agent to find an opening between the polymer chains of a network within a solution or hydrogel. The matrix is treated as an impenetrable boundary that is static relative to the motion of a diffusant. The diffusivity of a solute can, therefore, be expressed as the statistical probability of finding a series of these openings,

$$\frac{D_g}{D_0} = \int_{r^*}^{\infty} g(r)\, dr \qquad [8]$$

where, g(r) is the distribution function describing the distribution of the radii of openings between polymer chains, D_g is the diffusion coefficient of the agent in the gel or solution, D_0 is the free diffusion

coefficient of the solute in pure water, and r* is the critical limiting radius to permit solute passage. In 1958, Ogston developed an expression to define the distribution of openings between randomly oriented straight fibers of negligible width,[46]

$$g(r) = \frac{\pi r}{2R^2} \exp\left[-\frac{\pi}{4}\left(\frac{r}{R}\right)^2\right] \quad [9]$$

where R is the mean radius of the distribution. Polymer networks are not exactly straight fibers; however, this distribution was assumed to be a valid approximation of a transient polymer matrix (Figure 4). Substituting Equation 9 into 8 and carrying out the integration results in the following relationship,

$$\frac{D_g}{D_0} = exp\left[\frac{-\pi}{4}\left(\frac{r^*}{R}\right)^2\right] \quad [10]$$

Equation 10 can be revised to consider the finite thickness of the polymer chains,

$$\frac{D_g}{D_0} = exp\left[\frac{-\pi}{4}\left(\frac{r_s + r_f}{\bar{r} + r_f}\right)^2\right] \quad [11]$$

where, $\bar{r}$ is the average radius of the openings between polymer chains, r_f is the cross-sectional radius of the polymer chains, and r_s is the hydrodynamic radius of the diffusing agent. Applying scaling concepts by de Gennes, the average radius of the openings can be characterized by the correlation length ($\xi = 2\,\bar{r}$), resulting in the final expression,

$$\frac{D_g}{D_0} = exp\left[-\pi\left(\frac{r_s + r_f}{\xi + 2r_f}\right)^2\right] \quad [12]$$

Equation 12 represents the generalized form of the obstruction-scaling model. The relationship can be further defined using Equation 7,

$$\frac{D_g}{D_0} = exp\left[-\pi\left(\frac{r_s + r_f}{R_g\left(c^*/c\right)^{\nu} + 2r_f}\right)^2\right] \quad [13]$$

And for hydrogels, the concentration of the polymer is defined as a volume fraction,

$$\frac{D_g}{D_0} = exp\left[-\pi\left(\frac{r_s + r_f}{R_g\left(c^*/\Phi\rho_p\right)^{\nu} + 2r_f}\right)^2\right] \qquad [14]$$

where, Φ is the polymer volume fraction of the hydrogel and ρ_p is the density of the polymer. If the assumptions behind its derivation are reasonable, Equation 14 should be able to predict the spontaneous diffusion coefficients of solute in polymer solutions and hydrogels.

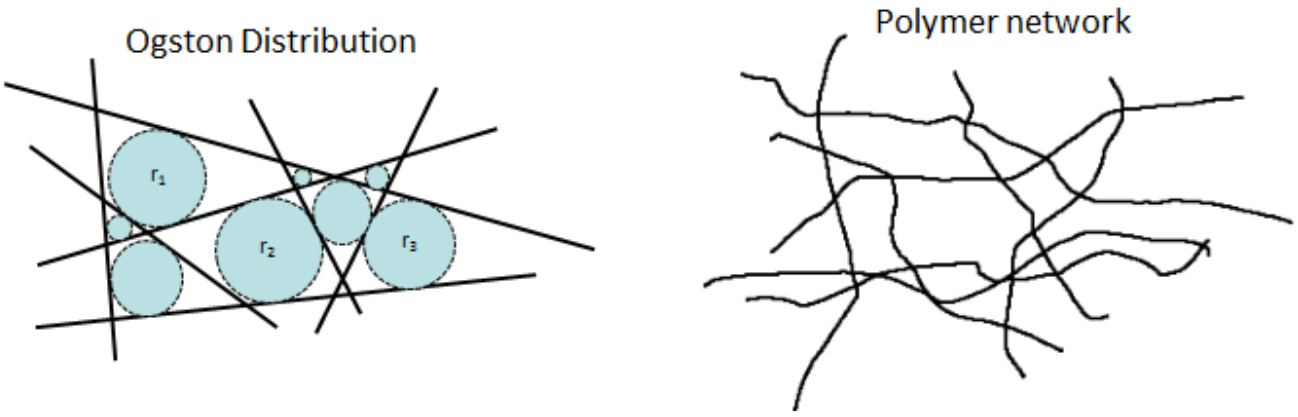

Figure 4: Ogston distribution

A concept image of a polymer network is portrayed as an assortment of entangled polymer chains that may be either a solution or hydrogel. The Ogston distribution simplifies the network by assuming that the chains are straight fibers of negligible width. r_i is the radius of the opening.

1.12 Obstruction-scaling diffusion model: assumptions

The assumptions of the obstruction-scaling model have been addressed elsewhere.[2,10,11,43] For clarity, the assumptions have been summarized. It is important to note that the assumptions documented in the original publication of the obstruction model were addressed to compensate for the scaling concepts developed by Schaefer.[2,44] Replacing these scaling methods with de Gennes' original argument reduced the overall number of parameters in the model and the degree of its derived assumptions,[11,12]

1) Polymer chains in solutions and hydrogels above their overlap concentration are assumed to form transient networks that are static relative to the mobility of the diffusant. The validity of this assumption was confirmed by Zhang and Amsden..[11]

2) Obstruction effects dominate the diffusion process in polymer solutions and gels in the absence of strong intermolecular interactions between the diffusant and the network. Hydrodynamic interactions are considered to be negligible. Electrostatic interactions between the network and the diffusant can be screened by electrolytes in the case of gels made with polyelectrolytes.[11]

3) The radius of the diffusing agent is approximated as a perfect sphere in the absence of reptation. Therefore, the Stokes' radius is roughly equivalent to the hydrodynamic radius of the diffusant.

4) The distribution of openings between polymer chains can be approximated by a random distribution of straight fibers. This assumption has been addressed in previous studies.[2,10,11,43]

5) Scaling relationships developed by de Gennes are appropriate methods for estimating the average distance between the polymers chains within a solution.[12]. This assumption was validated for polymer solutions in a study by Zhang and Amsden.[11] However, its application to hydrogels is directly correlated to the validity of assumption 6.

6) The correlation length of a hydrogel is the same as that of a polymer solution at equivalent concentrations. This assumption is unconfirmed and will be addressed in the sections that follow.

1.13 Measuring diffusion in hydrogels

The measurement of diffusion is an extensive topic that draws from a wide variety of disciplines. With the development and accessibility of new technologies, the complexity of measuring the movement of an agent within the boundaries of a given system is certainly less difficult now than it was in the past few decades. As new techniques emerge, the information that can be collected and extracted from a single diffusion experiment is becoming increasingly accurate. A very large number of techniques are available for measuring diffusion coefficients in polymer networks and so it was not possible to discuss all of them.

1.13.1 Release experiment

The release experiment is a classic technique that measures the concentration-time profile of the diffusing agent at perfect sink conditions.[47–49] It carries information on the mutual diffusion coefficient that can be extracted using models to describe the appropriate release mechanism for a system. Notable expressions were derived by Higuchi and Korsmeyer *et al.*.[50,51] These experiments are generally impractical for tracer measurements; however, maintaining the diffusant at low concentrations can generally render a chemical potential gradient negligible and simulate the self-diffusion phenomenon. This approach can determine tracer diffusion coefficients but is limited to global measurements.

1.13.2 Nuclear magnetic resonance

NMR measurements are typically carried out by observing the attenuation of the amplitudes of specific signals that describe the displacement of molecular agents along the z-direction.[11] Stack plots of the NMR spectra carry information regarding the tracer diffusion coefficients that can be extracted by fitting the appropriate mathematical model to the data.[11] Pulse field gradient (PFG-NMR) is often applied to polymer solutions and diffusion ordered spectroscopy (DOSY-NMR) to hydrogels.[11,52] Apart from the obvious equipment and experience limitations, according to Bengt *et al.*, the method is only applicable to diffusion systems with suitable spin echoes that are undisturbed by other spin echoes.[47]

1.13.3 Fluorescence recovery after photobleaching

Fluorescence recovery after photobleaching (FRAP) is an optical technique that exploits the photoannihilation properties of solute to measure diffusion in transparent systems like gels or solutions.[53] The technique has also been extensively used in biological disciplines to study the transport of proteins in cells and membranes.[54] In the presence of a high intensity laser, fluorophores may experience photon-induced chemical damage and covalent modification to permanently lose their observed fluorescence, often referred to as photobleaching.[55] This phenomenon is a real setback to microscopy imaging, but very useful to self-diffusion studies. As this is the primary technique used to measure diffusion in this study, the method will be described in greater detail.

FRAP measurements are bound to a user-defined region of interest (ROI) within a sample to observe the fluorescence-time profile of the boundary using confocal scanning laser microscopy (CSLM).[53] The fluorescently labeled molecules within the confines of the ROI lose their fluorescent capability upon excitation by a high intensity laser, selectively excluding those outside this region from bleaching.[53] The affected region is monitored using an attenuated laser to prevent further bleaching when recording. In the absence of strong intermolecular interactions between the fluorophores and their environment, the primary driving force for the recovery of the fluorescence signal within the ROI is tracer diffusion.[56] In other words, the active fluorophores displace the photobleached compounds as a result of the random thermal collisions occurring within the system (Figure 5). The intensity-time profile of the recovery period carries information on the tracer diffusion coefficient within the sample and may be extracted using models that describe the appropriate mechanism of recovery (Figure 6).[56] The technique is fast, non-destructive, and requires a small sample volume.[57] The method, however, has its limitations. For example, FRAP is sensitive to background noise in the form of unbound fluorophores and constrained to measuring transparent samples by its own optics. The viability of the method is largely dependent on the utility of the selected extraction model for which there are few models that are easy to solve.[53,58–60] A number of these models carry assumptions that may not fit the criteria for specific systems, in addition.

There are notable experience and cost barriers that characterize FRAP as less appealing in comparison to fundamental cases like the simulated self-diffusion observed in release experiments.[57] On the other hand, the advantages in using FRAP are often in its versatility. It may process localized measurements during cross-linking or compare regions of a heterogeneous system that may otherwise be difficult to measure.[55] FRAP's compatibility with processing a wide range of diffusion magnitudes (0.1-300 $\mu m^2/s$) is sufficient but limited to the CSLM's photobleaching capability.[53,61]

FRAP and NMR diffusion measurements are generally consistent; the choice of technique often reduces to accessibility, experience, and convenience.[62] In this study, FRAP was selected over NMR on several points. Firstly, the aim was to circumvent the limitations associated with using NMR tubes. Although seemingly trivial, the confined volume of the NMR vessel is difficult to prepare with a hydrogel that is weak or brittle without compromising the structure and integrity of the gel. As a result, experiments are often prepared by loading the solute during cross-linking within the confines of the vessel by photopolymerization, heating, or catalysis.[62] It is considered unfavorable to use this approach as the spatial distribution of the network during cross-linking may encapsulate the agent or initiate chemical interactions between the solute and the matrix, especially for proteins. Nevertheless, loading hydrogels into NMR tubes, however inconvenient, has been done rather successfully using cylindrical molds.[63,64] Secondly, measuring diffusion coefficients using NMR provides global measurements with limited information on the heterogeneous nature of a network, whereas with FRAP, it is a localized measurement confined to a user-defined boundary that may provide additional details on the consistency of the gel.[65] FRAP is a more sensitive method allowing lower concentrations of a probe to maintain a sufficient signal to noise ratio (S/N) that may, by extension, reduce the likelihood of molecular aggregation in the gel.[65] Lastly, selecting a technique that was new within the group was certainly a determining factor. The obstruction model, having already been subjected to NMR by Zhang and Amsden,[11] was strong incentive to investigate alternative methods like FRAP.

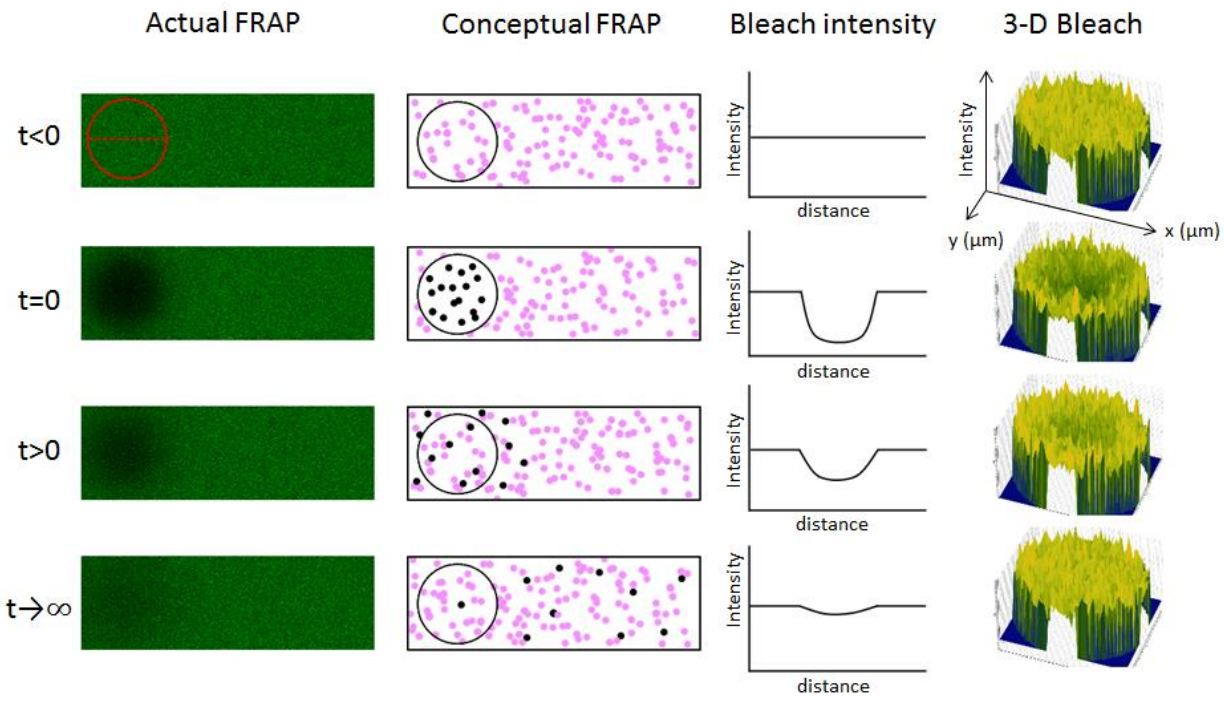

Figure 5: A typical FRAP experiment

The red circle represents the selected ROI. In this case, it happens to be a uniform disk. The actual FRAP experiment is measuring the diffusion of FITC-dextran within polymer solutions of sodium alginate; the images were taken at different time points throughout the experiment. The concept of tracer diffusion is portrayed in the conceptualized FRAP images, wherein the photobleached fluorophores diffuse out from the selected region due to Brownian motion in the absence of strong intermolecular attractions. The bleach intensity follows the horizontal (red, dashed) line within the ROI, illustrating the intensity distribution of a typical photobleach. At $t < 0$, is the prebleach phase, $t = 0$ is the start of the photobleaching sequence, $t > 0$ is the recovery phase, and as $t \rightarrow \infty$, full recovery is observed.

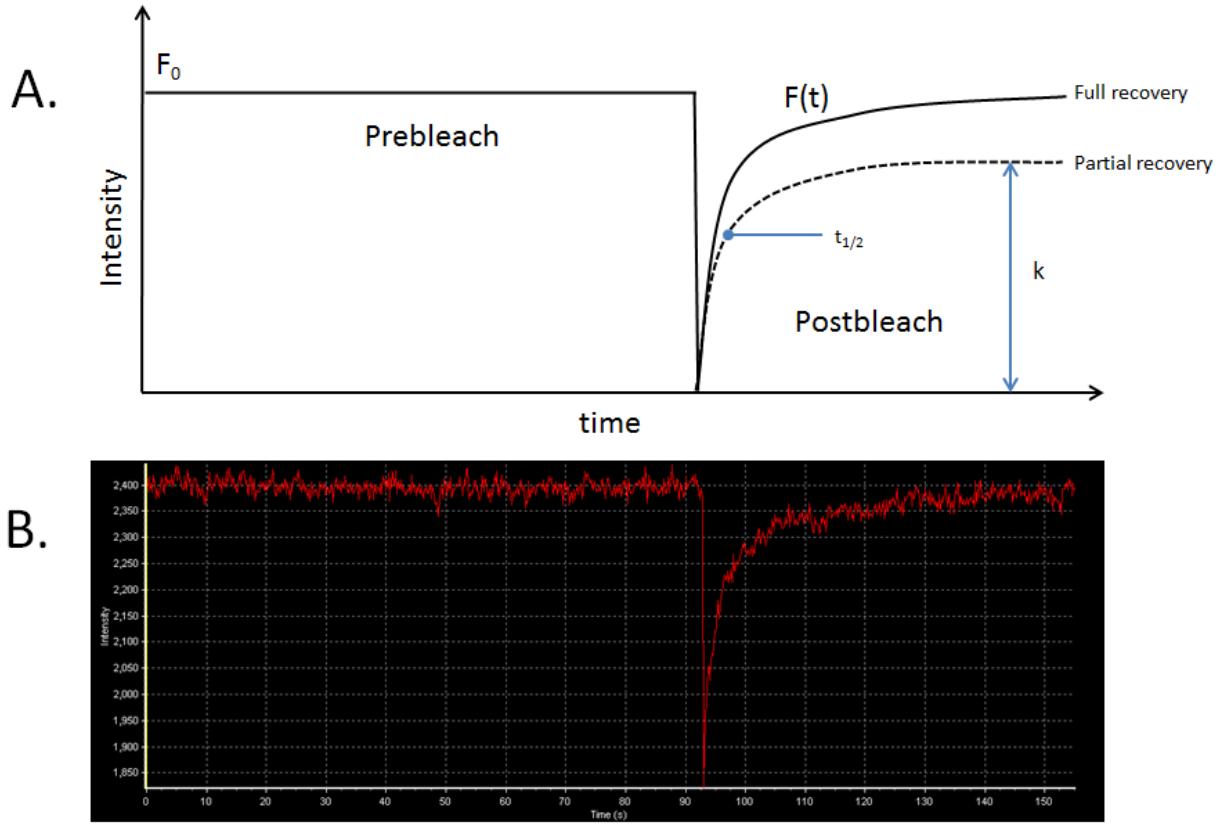

Figure 6: A typical FRAP recovery curve

A concept image of a typical FRAP recovery curve is conveyed in (A). The intensity time profile is described in respect to a full recovery (k = 1) and a partial recovery (k ≠ 1). The half time ($t_{1/2}$) for the full recovery curve is represented as the time in which half the fluorescence signal was recovered. An actual FRAP recovery curve is conveyed in (B) that was processed from the diffusion of FITC-dextran within a polymer solution of sodium alginate.

1.14 Fluorochromes

Fluorescence occurs when a species absorbs light of one wavelength and emits that of another.[66] This phenomenon is actually a rare occurrence in most compounds and may be induced by conjugating chemical fluorescent compounds called fluorochromes, otherwise referred to as fluorophores, to species that are of particular interest. Fluorochromes intrinsically respond to the electromagnetic radiation from an external source such as a laser by transitioning into an excited electronic singlet state, i.e. absorption.[66] This state is very short lived (1-10 nanoseconds) and will partially dissipate its energy in the form of an electromagnetic wave that is weaker than that of the absorbed and, therefore, longer in comparison.[66]

The resulting fluorescence is basically the release of a photon as the molecule returns to its ground state; however, not all excited fluorophores return to their initial state and may, occasionally, undergo a phenomenon known as quenching.

Fluorophores have a life cycle. They can be repeatedly excited for a specific number of cycles until exhausted, at which point they permanently lose their fluorescence. Photobleaching is a phenomenon that is thought to exploit this concept by either amplifying the absorption/emission process leading to fluorescence loss via exhaustion or by inducing the agent from a short-lived excited singlet state to a relatively long-lived excited triplet state that is chemically more reactive.[66] These photon-induced reactive species may result in covalent modifications that annihilate their potential fluorescence. Quenching is the result of similar interactions between fluorophores that may be in either an excited or grounded state, depending on the type of quenching, that likewise destroy the fluorescence of a fluorochrome.[66]

Fluorophores are often characterized by their quantum yield, an important parameter that determines how efficient their fluorescence is on a scale. The yield is described by the ratio of the photons emitted to the photons absorbed, i.e. high quantum yields provide increased fluorescence from a consistent source.[66] Agents like fluorescein isothiocyanate (FITC) and fluorescein are common fluorophores in science because of their high quantum yields.[65] In this study, FITC was selected to be the primary dye for FRAP due to its high quantum yield and its high susceptibility to photobleaching.

Chapter 2

Objectives and Specific Aims

2.1 Objectives

The primary objective of this study was to assess the validity of the assumption that the correlation length of a polymer network in the solution state is the same in the gel state at equivalent concentrations. This assumption remains unconfirmed and must be valid to extend the applicability of the obstruction-scaling model to hydrogels. The secondary objective was to investigate the model's capability to provide accurate predictions of the diffusion coefficient of a solute in a hydrogel.

2.2 Specific aims

The specific aim of this study was to establish a FRAP protocol that is compatible with commercially available confocal microscopes to measure the tracer diffusion coefficient of solute in different hydrogels within the assumptions and limitations of the method. This technique would be used to assess the validity of the correlation length assumption by comparing the spontaneous diffusion measurements of various fluorescently labeled dextran agents (4, 10, 20, and 40 kDa) in different hydrogels to the predictions of the obstruction model. A good fit between the observed and the predicted would suggest that the unconfirmed correlation assumption is appropriate. A detailed analysis of the fit would evaluate the utility that the model provides.

Chapter 3

Literature Review

3.1 Part I: Diffusion models

3.1.1 Maxwell-Fricke

The first obstruction model was introduced by Fricke in 1924,[40]

$$\frac{\mathrm{D}(1-\varphi)}{D_0} = \frac{1-\varphi^*}{1+\varphi^*/\chi} \qquad [15]$$

where, D is the spontaneous diffusion coefficient, D_0 is the diffusion coefficient at infinite dilution, φ is the volume fraction of polymer, and φ* is the volume fractions of polymer plus non-diffusing solvent bound to the polymer, and χ is a parameter depending on solvent shape. The Maxwell-Fricke model was derived on the assumption that a polymer network is an immobile and impenetrable suspension of chains within a mobile solvent continuum. It was generally suitable for describing systems in very dilute circumstances using small diffusing particles. In a study by Cheever *et. al.*, the model conveyed a good fit to the measured self-diffusion coefficients of water in polystyrene and silica solutions using NMR.[67] Cheever *et al.* compared the model to a very limited number of data measurements, making it difficult to assess the consistency of its predictions over a wide range of concentrations. The limitations of the expression become apparent at high volume fractions of polymer, notably for large diffusing agents as demonstrated in a study by Waggoner *et al.*.[68] Although often invoked, this equation is of little utility as it does not take into consideration the properties of the gel or the solute. The model, for example, cannot distinguish a difference in the radius between BSA (35Å)[11] and water (1.9Å).[10] In the same system, these two very different probes would have a similar normalized diffusion profile. The Maxwell-Fricke relationship should only be considered for the diffusion of small probes such as water or urea in the dilute

regime since, under these circumstances, the radius of the diffusant has a very small impact on the observed diffusion.

3.1.2 Mackie and Meares

An obstruction model was developed by Mackie and Meares in 1955 using the same concepts originally proposed by Fricke,[40,42]

$$\frac{\mathrm{D}}{D_0} = \left(\frac{1-\varphi}{1+\varphi}\right)^2 \qquad [16]$$

where, the parameters are identical to those defined in Equation 15. This model provides the same degree of utility as Equation 15 for which its applicability is limited to small diffusing agents. The model of Mackie and Meares is based on obstruction tortuosity and should be reserved as a more reliable method to predict diffusion coefficients in the same conditions as the Maxwell-Fricke model.

3.1.3 Ogston *et al.*

Ogston *et al*. developed a new approach to modeling solute diffusion in polymer networks in a study that was initially set out to provide a theoretical analysis for the empirical equation of Laurent *et al.*[41,69] The resulting obstruction expression was published in 1973,[41]

$$\frac{\mathrm{D}}{D_0} = exp\left(-\frac{r_s + r_f}{r_f}\varphi^{1/2}\right) \qquad [17]$$

where, r_s is the hydrodynamic radius of the diffusant and r_f is the cross-sectional radius of the polymer. The model of Ogston *et al.* was developed on the conceptual framework that solute diffusion in networks can be approximated by a succession of incremental jumps that will succeed in the absence of encountering any physical obstructions in the form of deflection by the polymer chains.[2] The polymer network within a solution or hydrogel was assumed to be a collection of randomly oriented straight chain fibers of negligible width using a distribution derived by Ogston in 1958.[46] In a study by Gagnon *et al.*,

the model was compared to the self-diffusion coefficients of different solute using PFG-NMR in high set curdlan hydrogels and demonstrated accurate predictions.[63] The diffusants were limited to a range between 3.3 Å to 4.9Å, making it difficult to assess its consistency using larger solute such as proteins. The polymer volume fractions in the study were also not varied. The limitations of the model became apparent in the comprehensive review by Muhr and Blanshard,[70] in which the expression demonstrated adequate predictions for small diffusing agents in gels, i.e. 3.0 Å or less, and provided poor fits to larger probes such as carbohydrates. In this study, it becomes obvious that the volume fraction of polymer alone is an inappropriate indicator of a hydrogel network's relative influence on the tortuosity of a diffusant. Low volume fraction hydrogels consisting of neutral polymers, for example, could have a greater diffusion-related impact than those of higher volume fractions, depending on their physical properties. The model of Ogston *et al.* was the first obstruction model to consider the solute radius; despite this, its use should be reserved for small diffusing agents in the dilute to semi-dilute regime.

3.1.4 Johansson *et al.*

The shortcomings of the model by Ogston *et al.* were attributed to its lack of consideration for the flexibility of polymer chains within a hydrogel or polymer solution, according to Johansson *et al.*.[71] Johansson and coworkers derived a new model derived on the work of Ogston *et al.* in 1991,[72]

$$\frac{\mathrm{D}}{D_0} = e^{-\alpha} + \alpha^2 e^{\alpha} E_1(2\alpha) \qquad [18]$$

where α is a grouped parameter,

$$\alpha = \varphi \left(\frac{r_s + r_f}{r_f} \right)^2 \qquad [19]$$

where, E is an exponential integral. The model of Johansson *et al.* was derived on several assumptions: (1) obstruction effects govern the diffusion of spherical solute within hydrogels and polymer solutions in

the absence of electrostatic interactions. Hydrodynamic interactions are negligible; (2) the polymer network is static relative to the mobility of a diffusant that is impenetrable and undisturbed by solute; and (3) the polymer network can be decomposed into cylindrical cells, where the contribution of each cell to the diffusion of a probe is determined by the distribution of spaces within the matrix. The average diffusivity within a cell can be determined by solving Fick's first law.[2] The global diffusivity of a solute is then calculated by summing up the number of cells having a given radius times the average diffusivity within that cell, for which the distribution of the cell radii was calculated using the Ogston distribution.[2,46] The model demonstrated a reasonable fit to the diffusion measurements of albumin in dextran and hyaluronic acid solutions in a study by Ogston *et al*..[41] Moreover, simulations of Brownian motion by Johansson *et al* were consistent with its predictions.[72] Bu and Russo demonstrated using FRAP that the model was inclined to underestimate the diffusion coefficients of high molecular weight dextrans in aqueous hydroxypropyl cellulose but provided good fits for those that were low.[73] This may be due to dextran's tendency to exhibit reptation within systems. The model of Johansson *et al*. should be reserved for the diffusion of small probes in the dilute and semi-dilute regime.

3.1.5 Cukier

The first hydrodynamic model was derived by Cukier in 1984 for semi-dilute polymer solutions,[74]

$$\frac{\mathrm{D}}{D_0} = exp(-\kappa r_s) \qquad [20]$$

and for dilute solutions,

$$\frac{\mathrm{D}}{D_0} = 1 - \kappa r_s \qquad [21]$$

where, κ is a hydrodynamic screening parameter. Cukier investigated relationships to the screening parameter for polymers that behave as rods within a network,

$$\kappa = \left(\frac{3\pi L N_A}{\ln(L/2r_h)M}\right)^{\frac{1}{2}} c^{1/2} \quad [22]$$

where, N_A is Avogadro's number, L is the length of the rod, c is the concentration of the polymer, and M is the molecular weight of the polymer. A relationship was then derived for polymers that behave as coils,

$$\kappa = (6\pi n_a{}^* a)^{1/2} \quad [23]$$

where, n_a* is the monomer number density and a is the monomer radius. Cukier demonstrated that the screening parameter can also be defined in relation to concentration using scaling concepts, i.e. $\kappa \sim c^{\nu}$,

$$\frac{D}{D_0} = exp(-kr_s c^{\nu}) \quad [24]$$

where, k is a constant of proportionality and ν is a scaling parameter. The scaling parameter was shown to vary in different studies at the time of this model's publication with plenty of controversy on its values.[32] The majority of publications are now in agreement with de Gennes' proposed scaling concepts that define ν = 1 for theta solvents, 0.5 for marginal solvents, and 0.75 for good solvents.[12] The model was derived on the concept that the polymer chains within a network are centers of hydrodynamic resistance that are static relative to the diffusion of a Brownian sphere.[2] The polymer chains enhance the frictional drag on the solute by slowing down the fluid near the chains.[2] The model by Cukier was shown to be consistent with the diffusion coefficients of water in different gelatin hydrogels in a study by Mel'nichenko *et al.* using slow neutron transmission methods.[75] In contrast, experiments by Park *et al.* via holographic relaxation methods demonstrate the limitations of Cukier's model for approximating the diffusion of larger agents like BSA in polyacrylamide (PA) hydrogels and suggested that the model was limited to small diffusing probes.[76] Rotstein *et al.* corroborated this limitation by comparing the model to tracer diffusion measurements of linear polystyrenes in poly(vinyl methyl ether) (PVME) hydrogels using dynamic light scattering (DLS) at high volume fractions of polymer.[77] However, polystyrene is likely not going to behave as a sphere within solution and is almost certain to experience the effects of reptation

within a system like a gel, especially at high volume fractions as was the case in the study. Rotstein *et al.* were outside the boundaries of Cukier's derived assumptions and naturally observed a poor fit. Care must be taken to interpret results within the limitations of each model; otherwise, the results are likely to be unrealistic and aptly lack any meaning. The effects of obstruction were no longer negligible at high volume fractions of polymer in these studies because the solute is likely to encounter deflection by polymer chains at high values of φ. The model by Cukier should only be considered for small diffusing agents in the dilute regime.

3.1.6 Altenberger *et al.*

Altenberger developed a hydrodynamic model in 1986,[35]

$$\frac{\mathrm{D}}{D_0} = 1 - Ac^{\frac{1}{2}} - Bc + \cdots \qquad [25]$$

where, A is proportional to the radius, i.e. $A \sim r_s r_f^{1/2}$, and B is a parameter that defines the interactions between the network and the diffusant. This expression was later generalized by the group,

$$\frac{\mathrm{D}}{D_0} = \exp(-\omega c^{1/2}) \qquad [26]$$

where, ѡ is a parameter depending on the diffusing particle. The model by Altenberger *et al.* demonstrated a striking resemblance to the model by Cukier, specifically Equations 25 & 21 and Equations 26 & 20. The latter two expressions were later determined to be equivalent by Kosar and Phillips despite having very different derivations.[78] The model of Altenberger provides the same utility as that of Cukier and should be applied in similar systems since they are bound by analogous limitations and assumptions. Kosar *et al.* demonstrated a larger validity domain for the model of Alternberger than that of Cukier's, i.e. accurate predictions at higher volume fractions of polymer. This result is likely circumstantial and not a direct result of the model's utility.[78]

3.1.7 Phillies

Phillies derived a universal scaling equation using hydrodynamic concepts in 1986,[36]

$$\frac{D}{D_0} = \exp(-\alpha c^{\nu}) \qquad [27]$$

where, α is a scaling prefactor and ν is a scaling exponent. The scaling parameter α should primarily depend on the solute, while the scaling exponent ν should depend on the polymer and, in some cases, on the molecular weight of the diffusant. It was found that $\alpha \sim M^{0.9\pm0.1}$ for macromolecular diffusants and $\alpha \sim r_h/a_o$ for smaller diffusants, where a_o is the distance of closest approach.[36] Empirical relationships were determined for α by Park *et al.*[76] and Gibbs *et al.*,[79] $\alpha = 3.03r_h^{0.59}$ and $\alpha = 3.2r_h^{0.53}$, respectively. Furthermore, ν should scale to 1 for low molecular weight diffusants and to 0.5 for high molecular weight diffusants, $\nu \sim M^{-1/4}$.[36] Although possessing a similar form to the models of Altenberger and Cukier, the Phillies model is derived on different assumptions, most importantly that the polymer chains within a network are not viewed as static in relation to the mobility of a solute. The model of Phillies is arguably more of an empirical relationship rather than a conceptual model and its derived parameters have been highly controversial since the model was first introduced in 1986. The dependence and meaning of its scaling relationships are often disputed throughout the literature.[32] In a study by Masaro *et al.,* the model of Phillies demonstrated excellent fits to the tracer diffusion profile of water in poly(vinyl alcohol) (PVA) solutions using PFG-NMR.[80] The model was also in good agreement with a study by Johansson *et al.*.[72] Kosar and Phillips demonstrated that the model provided a good fit to the diffusion of large proteins like BSA in different dextran solutions using holographic interferometry.[78] In a study by Modesti *et al.,* the model's predictions of biodipy B3932 in octane-swollen bimodal networks of poly(dimethyl siloxane) (PDMS) demonstrated a poor fit to the measured tracer diffusion coefficients obtained by fluorescence correlation spectroscopy (FCS), whereas terrylene diimide demonstrated a good fit.[81] This is somewhat unexpected because these are small probes in comparison to BSA and are generally considered to be more

compatible than those that are large. This inconsistency may be attributed to electrostatic interactions between the B3932 fluorophores in the absence of screening.

It is often disputed that the model is successful because of its unusual flexibility compared to other conceptual models, largely as a result of its vague parameters. Recently in 2006, Phillies published an extensive review on the scaling parameters for a variety of molecular probes and polymer solutions within the literature.[82] In this study, Phillies addressed the controversy on the model's unusual flexibility stating that it betrays the fundamentals of mathematics to assume that the model is providing accidental good fits since it is no more flexible than any other model with three free parameters.[82] The model of Phillies can be curve fit to nearly any diffusion profile which is certainly an appealing concept and probably the reason for its high invocation within the literature. The model is often utilized for its simplicity and notably its degree of versatility. Without knowledge on the scaling parameters or a means to identify them for a particular system, the expression cannot provide *a priori* predictions. This limits the utility of the Phillies model in comparison to others that may be solved *a priori*, at least to some degree. The model of Phillies provides limited information on the properties of the polymer network or the solute. Furthermore, the empirical relationships used to define the scaling parameters are often inconsistent between systems. The model should be reserved for small and large diffusing agents in the dilute and semi-dilute regime.

3.1.8 Fujita

The first free-volume model was developed by Fujita in 1961,[37]

$$\mathrm{D} = \mathrm{ARTexp}\left(-\frac{B}{f_v}\right) \qquad [28]$$

where, A is a proportionality factor, B is the minimum hole size required for diffusant displacement that depends only on the particle size but not on the temperature or polymer concentration, f_v is the average free volume per molecule, R is the universal gas constant, and T is temperature. The model of Fujita is based on the conceptual theory of Cohen and Turnbull to explain the process of diffusion in a liquid.[83]

The model was derived on several assumptions: (1) the diffusion process is governed by the redistribution of free volume pockets in which a solute occupy to move from one point in a polymer network to another; (2) the redistribution of free volume does not require energy; and (3) the diffusion process is enabled when the free volume pocket reaches a size that is greater than B. According to Zhu *et al.*, the model provides excellent predictions for the tracer diffusion coefficients of ketones in poly(methyl methacrylate) (PMMA) solutions obtained by NMR.[84] The limitations of the model were addressed by Xia and Wang in a study that measured the diffusion of camphorquinone and thymoquinone in several different polymers.[85] They demonstrated that Fujita's model was suitable for low volume fractions of polymer at low degrees of cross-linking and would often provide inconsistent predictions in highly cross-linked polymers. According to Xia *et al.*, the model was too simple to demonstrate accurate predictions at high cross-link densities because there was a substantial increase in the glass transition temperature that cannot be predicted by the linear concentration dependence of fractional free volume.[85] The model of Fujita should be reserved for the diffusion of small agents in the dilute regime.

3.1.9 Yasuda *et al.*

A free-volume model developed in 1968 by Yasuda *et al.* and was based on the concepts by Fujita,[86]

$$\frac{\mathrm{D}}{D_0} = \exp\left(-\frac{B}{f_v}\left[1 - \frac{1}{1-\varphi}\right]\right) \qquad [29]$$

where, f_v is the solvent free volume in the solvent. The model was derived on the assumption that the total redistribution of free volume within a polymer solution arises from both the solvent and the polymer, referred to as polymer jumping units. The free volume contribution by the polymer, however, is considered to be small in comparison and, therefore, the free volume in a solution depends mostly on the solvent. The model by Yasuda *et al.* was compared to the diffusion measurements of NaCl in different methacrylated polymers in its original publication using a variety of solvents, such as dioxane, acetone, ethylene glycol, and water with formic acid, for which the model demonstrated reasonable predictions.[86]

According to Petit *et al.*, a gradual deterioration in the predictions of the expression can be observed as the probes become larger as a result of the model's inability to compensate for chain flexibility.[80] In this study, the tracer diffusion coefficients of several agents such as Poly(ethylene glycol) (PEG) 400-4000 in PVA solutions were measured using NMR and compared to the predictions of the model. In a study by Hennink and coworkers, the limitations of free volume theory were addressed by comparing the predictions of a similar model developed by Hennink *et al.* to the diffusion measurements of proteins in dextran hydrogels using NMR.[87] According to the group, the limitations in free volume theory become apparent as the molecular agent approaches the average distance between the chains of a network. The effects of obstruction by the polymer chains and hydrodynamic drag under such circumstances are no longer negligible and free-volume theory alone cannot describe the process. The model of Yasuda *et al.* and that of Hennink *et al.* should be considered for the diffusion of small agents in the dilute regime.

3.1.10 Concluding remarks

Diffusion in hydrogels and polymer solutions is a complex process. Over the past few decades, there have been a number of relationships proposed to relate the diffusivity of an agent to the properties of the solute and the polymer network. Each model has its merits and limitations such that the application of a particular expression should be approached with care and, to be of any use, within the limitations of its derived assumptions. It is important to remember that the expressions reviewed are models and cannot fully describe the diffusion phenomenon in either gels or solutions, so there will always be variation among their use in the literature and inconsistencies/controversies will be common. In spite of this, substantial progress has been made in their utility and has resulted in a better understanding of the factors that influence the diffusion of solute in polymer networks. Each diffusion theory has demonstrated success in different circumstances, but a majority of the models reviewed were limited to small diffusing probes at low polymer volume fractions. After having reviewed the literature, it is evident that there is currently no correct model or theory that can describe the diffusion of a solute within a network. The true process is probably a combination of obstruction by the polymer chains and hydrodynamic drag between

the components. Although free volume concepts have demonstrated relative success, the models have largely fallen out of favour because of their unusual parameters that are often difficult to measure or correlate. The other theories are generally more invoked than that of free volume and, for this reason, were covered in greater detail in this review. A very large number of expressions have been derived in the literature and so it was not possible to review all of them. The interested reader may wish to explore the other free volume models of Vrentas and Duda,[88–90] Peppas and Reinhart,[91,92] Lustig and Peppas,[93] and Gao and Fagerness.[94]

It is often the simplicity, applicability, and utility of a model that governs the selection process. The fact remains that it is still impossible to identify the diffusion coefficient of a solute within the network of a hydrogel or polymer solution (*a priori*) using a general expression. This lack of a consistent relationship between the observed and the predicted limits the potential utility of hydrogels until such a relationship is derived.

3.2 PART II: FRAP models

3.2.1 Average bleached region models

FRAP experiments come in the form of a recovery curve. Most modern CSLM will provide software to analyze the recovery of a photobleached region within a sample both qualitatively and quantitatively. The resulting curve resembles a simple exponential function of the form,

$$\frac{\mathrm{F(t)}}{F_0} = 1 - be^{-t/\tau} \qquad [30]$$

where, F is the measured fluorescence at time t, F_0 is the initial fluorescence intensity, b is the fraction of bleached fluorophores, and τ is the characteristic recovery time, where $t_{1/2} = \tau \ln 2$. The characteristic recovery time can be related to the tracer diffusion coefficient when curve fit to a FRAP experiment. Axelrod *et al*. were the first to relate the diffusion coefficient to Equation 30 by suggesting that,[95]

$$D = \Upsilon\left(\frac{\omega^2}{4t_{1/2}}\right) \qquad [31]$$

where, D is the tracer diffusion coefficient, Υ is a correction factor that is generally 0.88 for a uniform bleach but may vary as a function between 1.1 to 3 if the sample is bleached with a Gaussian energy distribution, and w is the radius of the disk. The relationship by Axelrod *et al.* does not consider any properties of the photoannihilation experiment and, therefore, if the magnitude of the photobleach is rather undefined, the value of D becomes questionable.[61] This approach should be reserved as a comparison to other more comprehensive models as an initial guess or for information on the general magnitude of a diffusion coefficient.[61]

A majority of earlier models were developed for stationary beams. A few models have been derived since then for appropriate use with the scanning beam of a confocal microscope. A model that has gained widespread interest for its accessibility was developed recently in 2003 by Braeckmans *et al.,* originally coined the uniform disk model (UDM) for its restrictions to uniform bleaching disks.[53] The model was then extended by the same group in 2011 using a more generalized approach to compensate for smaller disks in a study by Smisdom *et al.*, coined the generalized disk model (GDM).[56] These two models were derived on similar concepts that were originally proposed by Blonk *et al*. in a study that was predominately responsible for bringing FRAP to the CSLM in 1993.[96] Mathematical FRAP models that are based on averaging the bleach, i.e. UDM, provide a strong signal to noise ratio at a penalty to a loss of information by disregarding individual pixels. The models of Braeckmans *et al.* and Smisdom *et al.* will be reviewed in the methods that follow.

3.2.2 Pixel based models

The benefit of using average bleached region models is that they are generally straight forward in their derivation and do not require a series of complex computations. Models like the UDM or GDM are more conceptually appealing to the average FRAP user than pixel based models that take into

consideration the influence of every pixel within a given ROI. A limitation to averaging the bleach is that a large portion of the information is removed once the region is averaged. For this reason, several models have been developed on a pixel basis, often regarded to be the more accurate approach. The application of pixel based models is typically more intensive and their respective solution algorithms require software with high computation power or image processing capability. A recent pixel model was developed by Deschout *et al.* in 2010 that utilizes a rectangular bleaching geometry to quantify the tracer diffusion coefficient of a compound.[97] The model was recommended as an improved expression to the UDM; however, its restraint to rectangular regions limits the model to traditional raster scanning without an opportunity to apply the tornado scan, a CSLM function to be discussed in the sections that follow. The rFRAP method, as it was originally coined, has no dependency on the size of the rectangular region, making it a more flexible method than the UDM. Other FRAP models include maximum likelihood and spatial analysis. Maximum likelihood methods are dependent on statistical models to estimate the parameter of D from a typical recovery curve.[61] Spatial analysis methods rely on spatial statistics to correlate certain properties as a function of length in a material structure to estimate D.[61] These statistical models are rarely invoked as a result of their complexity and less appealing conceptual framework and will not be reviewed. FRAP models have also been developed to consider binding kinetics and reaction kinetics within biological disciplines.[60]

3.2.3 Concluding remarks

The progress of FRAP has largely been hindered by a few points. Firstly, FRAP relies on costly equipment that only recently became accessible, which has led to little incentive to further the accessibility of extraction models for the technique. As a result, accurate FRAP remains challenging for non-specialists. Secondly, a lack of well-defined protocols within the literature makes it difficult to grasp the general procedure of the technique, often overcomplicating an otherwise straightforward process. Lastly, FRAP is in its early stages of development with the technologies that have only been recently compatible with the method. In due time, the technique will become more practical.

Chapter 4

Materials and Methods

Unless otherwise stated, the methods described were conducted at a temperature of 25°C (SATP) and all materials were used as received.

4.1 Sodium alginate methacrylation via 2-aminoethyl methacrylate

Methacrylated alginate (MALG) was prepared by reacting sodium alginate with 2-aminoethyl methacrylate as described by Jeon *et al.*.[98] Sodium alginate (Protanal LF 10/60, MW 126,000), isolated from *Laminaria Hyperborea* stipe (F_G = 0.69; F_{GG} = 0.56)[99], was kindly donated by Pronova, Drammen, Norway. To prepare MALG, 4.0 g sodium alginate was dissolved in 0.2 L deionized water (Millipore Milli-Q Plus, 18 mΩ*cm) over the course of a few hours by vortex. The resulting solution was diluted with a morpholine buffer to prepare a 0.4 L mixture comprised of 1% sodium alginate (w/v), 0.5 M NaCl (Fisher Scientific), and 50 mM 2-morpholinoethanesulfonic acid (MES, Fisher) at pH 6.5. To activate the carboxyl moieties on the native alginate, 1.06 g N-hydroxysuccinimide (NHS, Acros Organics) and 3.50 g N-(3-dimethylaminopropyl)-N'-ethylcarbodiimide hydrochloride (EDC, Acros Organics) were dissolved in the alginate solution; the activation reaction was conducted under constant agitation for five minutes at pH 6.5. After five minutes, 1.52 g 2-aminoethyl methacrylate hydrochloride (AEMA, Polysciences) and 50 ppm hydroquinone monomethyl ether (MEHQ, Sigma Aldrich) were added to the amine-reactive alginate and the reaction was maintained at the preceding activation conditions for an additional 24 hours in the absence of light. The reagents had the following molar ratios: [ALG:EDC:NHS:AEMA] = [1.0:1.1:0.45:0.45].

4.2 Methacrylated alginate purification

Following section 4.1, the unrefined product (0.4 L) was admixed with a phosphate buffer to prepare a 0.6 L solution of 0.5 M sodium dihydrogen phosphate (Sigma Aldrich) that was left stirring for 24 hours

at pH 5.0 in the absence of light.[100,101] The resulting mixture was purified by dialysis (MWCO: 3500, Fisherbrand) against 4.0 L deionized water for 4 days (medium replaced at 2, 4, 8, 24, 48, 72, 96 hours), vacuum filtered (Whatman 42, Nalgene 0.2 μm RapidFlow Thermo Scientific), frozen, and lyophilized.

4.3 Molecular weight of methacrylated alginate

The molecular weight of the methacrylated alginate was calculated from the extent of methacrylate substitution introduced on the polymer chain on the basis of the weight average molecular weight of the native alginate samples. The methacrylation substitution was determined using ^{1}H NMR spectra obtained on a Bruker Avance-400 spectrometer equipped with a BBFO probe. The MALG was dissolved at 30 mg/mL in deuterium oxide, placed into an NMR tube, heated to 353 K, and subjected to analysis. The molecular weight of the alginate was calculated to be 134,000 g/mol, roughly a 6% difference from the native alginate.

4.4 Preparation of hydrogels via photopolymerization

Hydrogels were cross-linked via UV-initiated free radical polymerization using 2-hydroxy-1-[4-(2-hydroxyethoxy) phenyl]-2-methyl-1-propanone (I2959, Sigma Aldrich) as a catalyst. To prepare the gels, MALG was dissolved in a morpholine buffer comprised of 0.01 M MES, 0.22 M NaCl, 0.01% w/v sodium azide (Sigma Aldrich) and 4.5 mM I2959 at pH 7.2 over the course of a few hours while stirring. The resulting solution was centrifuged at 3000 rpm for 2 minutes (Centra CL2 Thermo Scientific IEC), poured into a mold (Lab-Tek Chamber Slide, 16 well x 0.15 cm^3), and photopolymerized (Figure 7) using UV light (365 nm) at 35 mW/cm^2 for 4 minutes (Hamamatsu LC8 Lightning Cure). The volume fraction of alginate in the hydrogels was varied by adjusting the concentration of the MALG in each batch and would range from 0.5-4.0% w/v. Hydrogels were purified in a 4.0 L buffer solution of 0.01 M MES, 0.22 M NaCl, and 0.01% sodium azide at pH 7.2 for 72 hours. The buffer solution was not changed.

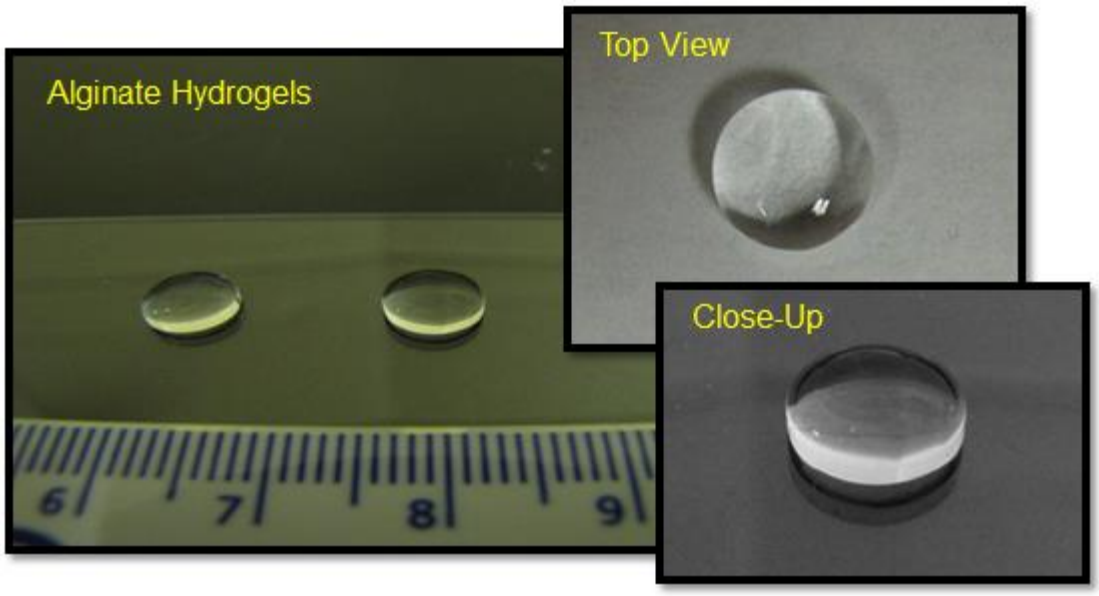

Figure 7: Alginate hydrogels

The hydrogels portrayed were formulated at 2% w/v. They were somewhat brittle. These hydrogels were cleaned and ready to undergo FRAP. However, the gels have yet to be loaded and have no fluorophore.

4.5 Polymer volume fraction

The volume fraction of polymer (Φ) was determined using a mass balance and the following equation,

$$\Phi = \frac{V_P}{V_g} = \frac{m_p \rho_g}{\rho_p m_g} = \left(\frac{m_p}{m_g}\right) \nu_p \qquad [32]$$

where, V is volume, m is mass, ρ is density, subscript p is the polymer, subscript g is the gel, and ν_p is the specific volume of the polymer ($\rho_g = \rho_{water}$). Hydrogels were weighed when wet, frozen, lyophilized, and then weighed when dry. The dry weight of a single gel was adjusted for any salts in its structure (m_p) and then multiplied by the specific volume of the polymer – (0.60 cm^3/g).[49] This value was divided by the hydrogel's weight when swollen to equilibrium (m_g), yielding the volume fraction of alginate in the gel, assuming that the density of MALG at 13% methacrylation is comparable to native alginate (1.66 g/cm^3).

4.6 Polymer chain radius

Using small-angle X-ray scattering (SAXS), the cross-sectional bare chain radius of sodium alginate has been determined by Wang *et al*. to be 0.55 nm.[102] This value was adjusted to include a water layer

upon polymer hydration by adding the diameter of a water molecule (0.28 nm) to the measured radius.[11] The resulting chain radius (r_f) was calculated to be 0.83 nm. The polymer chain radius of the MALG was evaluated by using a mole-weighted average of the radius of alginate residues and the radius of methacrylated alginate residues by applying the following expression,[10]

$$r_f = \left(\frac{M_m \nu_p}{l\pi N_A}\right)^{\frac{1}{2}} \quad [33]$$

where, M_m is the molecular weight of the monomer, l is the specific length of the monomer, ν_p is the specific volume of the polymer and N_A is Avogadro's number. The average radius for the MALG was estimated to be 0.84 nm, yielding a negligible difference between the native and the modified polymer. For the gels, the methacrylate groups were assumed to be at cross-link points and would not influence the chain radius. As a result, the cross-sectional polymer chain for the hydrogels was selected to be 0.83 nm.

4.7 Polymer radius of gyration

The radius of gyration (R_g) for Protanal LF 10/60 has been determined by Donati *et al.* to be 56.9 nm using high-performance size-exclusion chromatography coupled with multi-angle laser light scattering (HPSEC-RI-MALLS) for which the eluent was prepared using 0.05 M Na_2SO_4 and 0.01 M ethylenediaminetetraacetic acid (EDTA) at pH 6.0.[99] The viscosity of sodium alginate is largely unaffected over the range of pH 5-11; however, below pH 5 the carboxyl groups become protonated and electrostatic repulsion between the chains is reduced.[103] Excluding minor contributions by the EDTA and sodium alginate, the ionic strength (I) of the eluent used in the experiment by Donati *et al.* was estimated to be 0.15 M using the following expression,

$$I = \frac{1}{2}\left(\sum_{1}^{n} c_i {z_i}^2\right) \quad [34]$$

where, c is the molar concentration of the ions and z is the their respective charge. The buffer used in all FRAP experiments was comprised of 0.01 M MES, 0.22 M NaCl, and 0.01% sodium azide at pH 7.2, resulting in an ionic strength of 0.22 M if minor contributions by the sodium alginate, sodium azide, and MES are excluded. Assuming that the majority of the electrostatic interactions between the polymer chains are effectively screened at 0.15 M, [11] the radius of gyration of the alginate should not change at 0.22 M or pH 7.2.[11] Therefore, the radius of gyration for the native alginate was selected to be 56.9 nm. To determine the radius of gyration of the modified alginate, a curve-fitting procedure was applied to its measured diffusion profile. The R_g for the MALG was calculated to be 52.5 ± 3.0 nm.

4.8 Polymer correlation length

The correlation length of a network (ξ) was taken to be given by the following relationship,[12]

$$\xi = R_g \left(\frac{c^*}{c}\right)^{\nu} \qquad [35]$$

where, R_g is the radius of gyration of the polymer solution, c* is the overlap concentration of the polymer, c is the concentration of the polymer solution, and ν is a scaling parameter. The scaling parameter for sodium alginate was determined by Wang *et al.* to be 0.5 using SAXS, thus water is a marginal solvent. At 13% methacrylation, the physical properties of the MALG were assumed to be comparable to the native alginate and the scaling parameter was, therefore, selected to be 0.5 for the modified alginate.

4.9 Polymer overlap concentration

The overlap concentration (c*) of the alginate was determined by the following expression,[12]

$$c^* = \frac{3M}{4\pi N_A {R_g}^3} \qquad [36]$$

where, M is the molecular weight of the polymer, N_A is Avogadro's number, and R_g is the radius of gyration of the polymer.

4.10 FITC-dextran

To investigate the tracer diffusion of incorporated solute, the hydrogels were loaded with different dextran fluorophores (4, 10, 20, and 40 kDa molecular weight) by soaking them in a buffer solution of 0.01 M MES, 0.22 M NaCl, 0.01% sodium azide, and 1 mg/mL FITC-dextran (FDX) at pH 7.2 for two days in the absence of light. The concentration of the FITC-dextran was well-within the limits of the concentration range in which a linear relationship exists between the final fluorescence signal and the concentration of the agent, as verified in the study by Braeckmans' *et al*. [53] Polymer solutions were prepared by dissolving sodium alginate and MALG (5, 10, 15, and 20 mg/mL) in separate buffer solutions equivalent to the loading buffer for the gels and were then admixed with FDX-20. These solutions were stored for two days alongside the hydrogels in the absence of light during their loading to ensure consistency in the methods. The solutions containing FDX-20 were used to measure the radius of gyration of the modified alginate.

4.11 FITC-bovine serum albumin

To assess the validity of the calibration for the photobleaching disk used in the FRAP experiments, test solutions of native alginate (5, 10, 15, and 20 mg/mL) were prepared in a buffer of 0.01 M MES, 0.22 M NaCl, 0.01% sodium azide, and 4.0 mg/mL FITC-BSA at pH 7.2. The applicability of the method was investigated by comparing the measured tracer diffusion coefficients of FITC-BSA in test solutions via FRAP to the measured tracer diffusion coefficients obtained by Zhang and Amsden via PFG-NMR.[11] The diffusion measurements between the techniques should be consistent if the calibration is appropriate. Prior to using FITC-BSA, the linear concentration profile of the chromophore was analyzed by measuring the intensity of its fluorescence in buffer solutions containing different amounts of the agent (1-4 mg/mL) and prepared in accordance with the buffer used in the calibration test solutions. The concentration for the

FITC-BSA was selected to be 4.0 mg/mL, roughly at the upper limit of the linear concentration range, to compensate for the naturally faint signal of this probe; thereby, ensuring that the calibration experiments would provide sufficient fluorescence and still remain within the limitations of the profile.

4.12 FRAP equipment

The FRAP experiments were performed on an Olympus FluoView-1000 confocal scanning laser microscope using a 10x objective lens (UPLSAP010x, NA 0.4) in the absence of a simultaneous scanner. The 488 nm multi-line argon laser (30 mW) was the primary line used for excitation of the FITC-labeled fluorophores and their emitted fluorescence was detected using a 510-550 nm band pass filter. Photoannihilation of the sample was carried out by using a combination of the 488 and 405 nm lasers (50 mW, 80 mW total) set to full intensity. A custom imaging slide was prepared by using a polystyrene petri dish (Fisherbrand 60 x 15 mm) that was modified with a 0.17 mm (standard #1.5) glass cover slip in accordance with the specifications of the CSLM (Figure 8).

4.13 FRAP settings

All FRAP measurements were conducted using the FV-10 ASW ver. 3.0 software package provided by Olympus. The sample was first secured on to the stage of the CSLM and brought into focus at a depth that extended 100 µm from the surface of the glass cover slip. The FITC dye was then selected from the chromophore database and the confocal aperture opened to 80 µm or 1 airy unit for optimal sectioning. The intensity of the 488 nm laser line was initially set to 10% and then subsequently decreased in succession with a gradual increase in the high voltage (HV) to balance low power illumination with fluorescence detection. The high voltage was limited to 700 volts to avoid introducing additional noise. Using this approach, the laser line was generally configured to 2% of its full power, thereby providing a strong fluorescence signal and adequate attenuation to minimize the effects of bleaching when recording. The gain was set to a multiplier of 1.0 and remained as such for the duration of all FRAP experiments. The offset was observed to have an influence on the photobleaching capability of the CSLM at high levels

and remained at 0 to ensure consistency between samples. FRAP measurements were carried out after drawing a disk of specific diameter in the bleaching software by selecting the tornado scan in preference to the standard raster scan (Figure 9). The diameter of these disks was determined by a simple calibration protocol that fits the size of the ROI to a known free diffusion coefficient for a specific fluorochrome. The image acquisition settings were set to capture 800 frames total (200 pre-bleach and 600 post-bleach) with the photoannihilation sequence fixed at 110 ms for all measurements, unless specified otherwise. Additional settings such as zoom factor and image resolution were set to 7x and 320x320 pixels, respectively; however, the user-defined field of view was cropped by 80-90% to increase the frame rate, resulting in up to ~10 frames/second using a unidirectional scan.

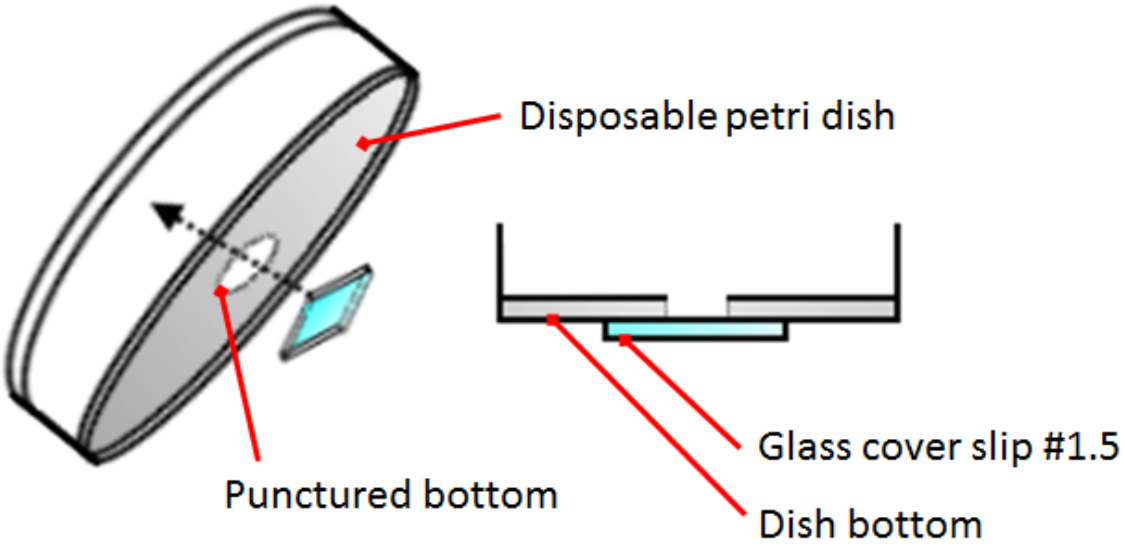

Figure 8: Customized imaging slide

The glass cover slip was fixed on to the bottom of the petri dish with a combination of high vacuum grease (Dow Corning) and quick set epoxy (Super Glue). The dish was first perforated by heating a steel cylindrical punch and boring the plastic bottom; the puncture was then sanded and leveled to a smooth surface prior to applying the cover slip.

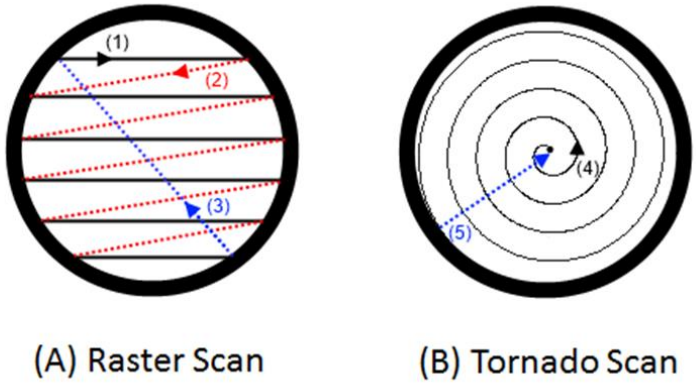

Figure 9: Tornado scan vs. Raster scan

Starting from the top-left and going to the bottom-right, the high intensity laser is turned on one line at a time (1) and switched off as it proceeds towards the next line (2) in the raster sequence (A). Once the scan is complete, the laser will make its way to the beginning of the first line and repeat the cycle (3). The tornado bleach (B), in contrast, starts from a central point and proceeds to scan in a helical pattern until reaching the edge of the defined ROI (4); it is switched off as it repositions to the starting point to repeat the sequence (5). The raster scan is often unidirectional as depicted above; however, newer microscopes may provide a bidirectional option generally at a cost to the signal to noise ratio of the experiment. The tornado bleach eliminates the downtime that a conventional raster scan will experience by reducing the cycle time of a complete scan and, in accordance, generates a quicker photobleach in comparison to the raster bleach. Fluorophores at the very edge of the disk are more susceptible to migrate out of the ROI during photoannihilation and contribute to bleaching during acquisition as a result of their position. This phenomenon is more influential in conventional raster scans because the bleach is initiated and completed at the edge of the disk as the sequence proceeds. By reducing unnecessary scanning and capitalizing on bleach efficiency, the tornado bleach is better suited for regions such as perfect disks, whereas the conventional raster scan is more appropriate for squares, rectangles, straight lines, and other user-defined regions of interest.

4.14 ROI calibration

To calibrate the ROI, the molecular probe was dissolved in deionized water at a concentration that remains below the upper limit of its linear profile, filtered by syringe (0.22 µm, Fisherbrand), centrifuged at 3200 RPM for 30 seconds, and injected into the well of the customized FRAP dish. The well was covered with a glass cover slip that was coated with a thin layer of vacuum grease to generate a strong seal between the slip and the petri dish to minimize the effects of flow. The sample was then secured to the stage of the CSLM and allowed to reach equilibrium once a position (x,y,z) has been locked into the system. From this point forward the mechanical stage was only ever repositioned within

the software using micron-scale increments to avoid introducing convective flow by sudden movements. The diameter of the ROI was then calibrated to a diffusion coefficient at infinite dilution for a specific fluorophore prior to proceeding with image acquisition or photobleaching. As an initial approximation, the radius of the bleaching disk was intentionally set too high i.e. 30 μm; its recovery curve was processed and the resulting diffusion coefficient was then compared to other coefficients in the literature. The diameter of the ROI was adjusted if the measurement was inconsistent with the literature coefficients and this led to a continuous cycle of adjustments until the observed measurements were dependable. The measured diffusion coefficient and the size of the ROI exhibited a positive correlation in all cases. The calibration method was validated by comparing the measured diffusion coefficients obtained by FRAP to measurements by Zhang and Amsden via PFG-NMR on different sodium alginate solutions.[11]

4.15 Data extraction and fitting

FRAP data were obtained using the FV-10 ASW ver. 3.0 software package provided by Olympus. The data extraction was carried out by collecting the fluorescence intensity for each image within a stack over the time frame of a single FRAP experiment for the photobleaching disk and its reference region, essentially an exact copy of the ROI in a location that is not affected by the photoannihilation sequence. The distance between the two regions was sufficiently large to avoid influence from either signal. The FRAP model initially selected was the generalized disk model (GDM) derived by Smisdom *et al.*,[56]

$$\frac{F(w,t)}{F_0(w)} = 1 - K_0\left\{1 - e^{-\zeta}[I_0(\zeta) + I_1(\zeta)]\right\} \qquad [37]$$

where, ζ is a grouped parameter,

$$\zeta = \frac{w^2}{\left(\frac{r_d^2}{4}\right) + 2D[t + (r_b^2/8D)]} = \frac{w^2}{2Dt + R} \qquad [38]$$

where, F is the fluorescence of the disk of size w at time t, F_0 is the fluorescence in the disk prior to photobleaching, K_0 is a photobleaching parameter, I_0 and I_1 are the modified Bessel functions of zeroth and first order respectively, w is the radius of the disk, t is time, r_b is the resolution of the bleaching beam, r_d is the resolution of the image, R is a grouped parameter dependent on the bleach, and D is the tracer diffusion coefficient of the agent. When w >> R, the generalized disk model reverts back into the uniform disk model (UDM) derived by Braeckmans *et al.*.[53] The bleaching parameter R was initially extracted by global curve fitting the GDM to FRAP experiments (5 or more) that varied by the size of their ROI and was found to be negligible in nearly all cases, suggesting that the disks were of large enough diameter to apply the UDM as an extraction tool. Furthermore, to account for a mobile fraction in the recovery phase, the following relationship was used,

$$F(w,t) = k\frac{F(w,t)}{F_0(w)} + (1-k)\frac{F(w,0)}{F_0(w)} \qquad [39]$$

where, k is the mobile fraction and (1-k) the immobile fraction. The data collected from a typical FRAP experiment comes in the form of a recovery curve and that was normalized using the following equation,

$$F_r(t) = \frac{I(w,t)}{I_{pre}(w)}\frac{R_{pre}(w)}{R(w,t)} \qquad [40]$$

where, I is the fluorescence of the primary disk of size w at any time t, I_{pre} is the average fluorescence prior to photobleaching of the primary disk, R is the fluorescence of the reference disk of size w at any time t, R_{pre} is the average fluorescence prior to photobleaching of the reference disk, and F_r is the normalized fluorescence. The UDM was used as an extraction model to gain information on the tracer diffusion coefficient of solute within hydrogels and polymer solutions by curve fitting Equations 37 & 39 to the normalized recovery of a typical FRAP experiment using a GRG non-linear least squares algorithm, for which the fitted parameters were collectively: k, K_0, and D, k = 1 for complete recovery (Figure 10).

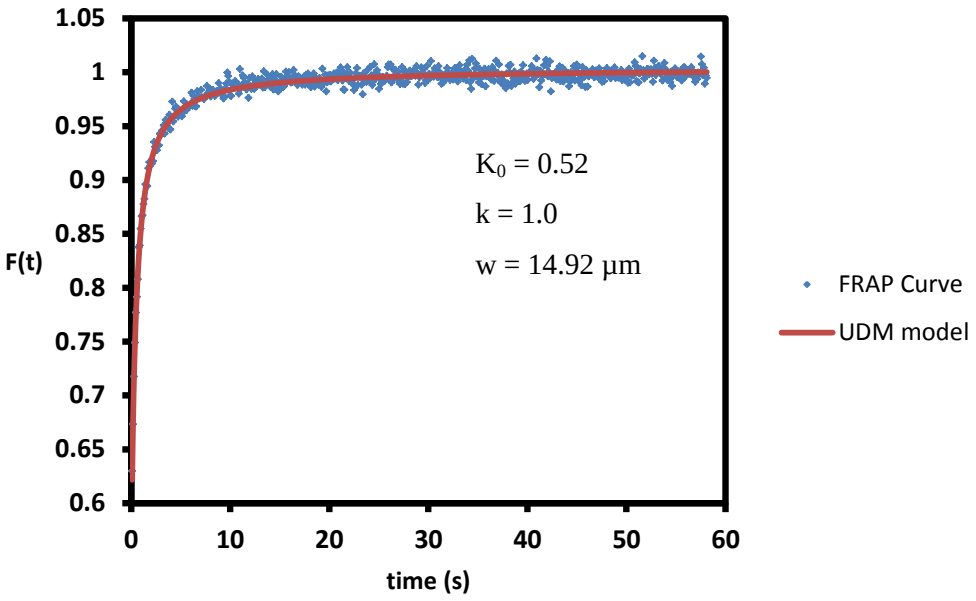

Figure 10: Curve fitting the UDM to a typical recovery curve

The figure conveys the diffusion of FITC-dextran in a methacrylate-alginate hydrogel. The experiment reaches full recovery (k = 1), which suggests that there was little to no interaction between the diffusant and the network.

Chapter 5

Results and Discussion

5.1 Radius of gyration of the modified alginate

The radius of gyration of the MALG was calculated using a curve-fitting procedure (Figure 11),

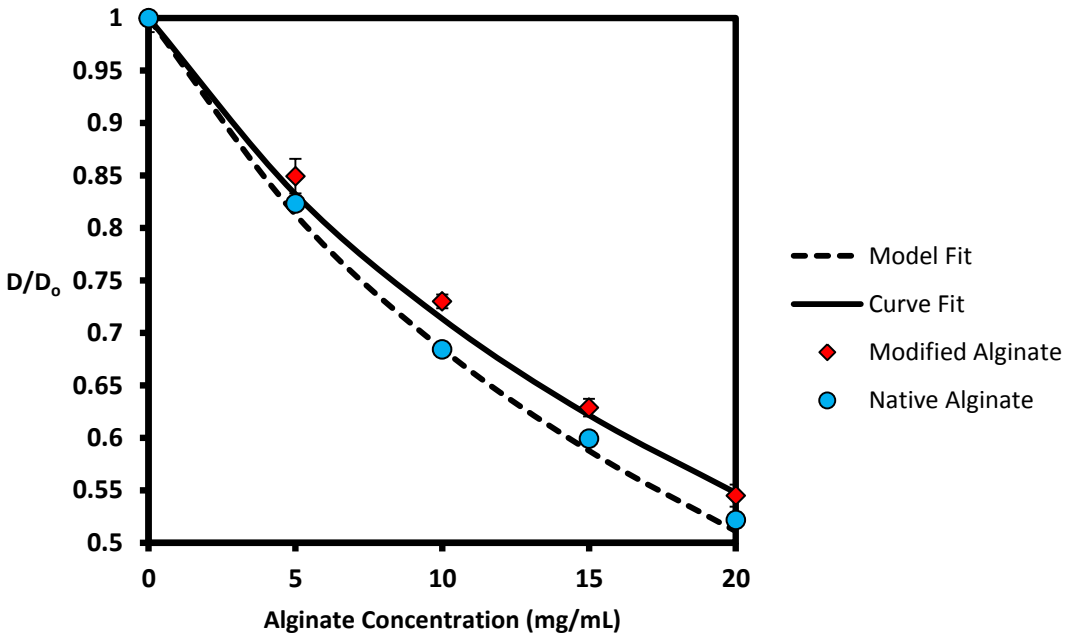

Figure 11: Comparison of the diffusion profile of the native alginate to the MALG

The data illustrates the results of two independent experiments. In the first experiment, the tracer diffusion coefficients of FDX-20 were measured in different solutions of native alginate using FRAP. These experimental diffusion coefficients (blue circles) were then plotted in comparison to the diffusion coefficients estimated by the obstruction-scaling model (dotted line). The results show a strong relationship between the observed and the predicted, conveying the prediction capability of the obstruction model for alginate solutions. In the second experiment, FRAP measurements were repeated using FDX-20 in different solutions of MALG, and the results (red diamonds) demonstrate a noticeable, but slight, difference in the diffusion profiles between the two polymers. This result inferred that the

physical properties of the MALG were different than those of the native alginate and would need to be identified to apply the model to gels.

The radius of gyration was calculated by using the obstruction expression to extract information from the measured diffusion coefficients of the modified alginate. The obstruction model was curve fit to the diffusion profile of the MALG (red diamonds) using a standard least squares (non-linear) fitting algorithm in Graphpad Prism 6 (solid line). The excellent fit of the model to the native alginate suggests that curve fitting is a viable approach for extracting this new parameter. Each data point is an average of at least three diffusion measurements and the error bars indicate the standard deviation. The new R_g was calculated to be 52.5 ± 3.0 nm at a 95% confidence interval, roughly an 8% difference from the unmodified alginate. It is reasonable to assume that the observed decrease in R_g stems from a fluctuation in the polarity of the chains as a result of the methacrylate groups, resulting in modified chains that were slightly less inclined to interact with the medium. In a study by Donati *et al.,* a noticeable decrease in the radius of gyration was observed for the modification of the same alginate, Protanal LF 10/60 of the same molecular weight, using galactose substitution.[99] According to the group, the drop in R_g was the result of a reduction in chain flexibility due to a change in the conformational space available to the affected monomers. However, the observed decrease in R_g of the methacrylate-substituted alginate is likely dominated by the polymer-solvent interactions and not steric effects.

5.2 FITC-BSA linear concentration profile

The concentration of the FITC-BSA was selected to be 4.0 mg/mL to balance low power illumination with high fluorescence detection. Lower concentrations, although linear, would need to be adjusted with an increase in the intensity of the 488 nm laser line, often resulting in significant photobleaching. In the UDM, the pixel intensity changes of a dissolving disk are correlated to the concentration changes of the probe. The relationship between pixel intensity and concentration must be linear for a fluorophore like FITC-BSA to be appropriate for use in FRAP. This linear profile was necessary to validate the disk calibration in FRAP and it was developed using the CSLM (Figure 12),

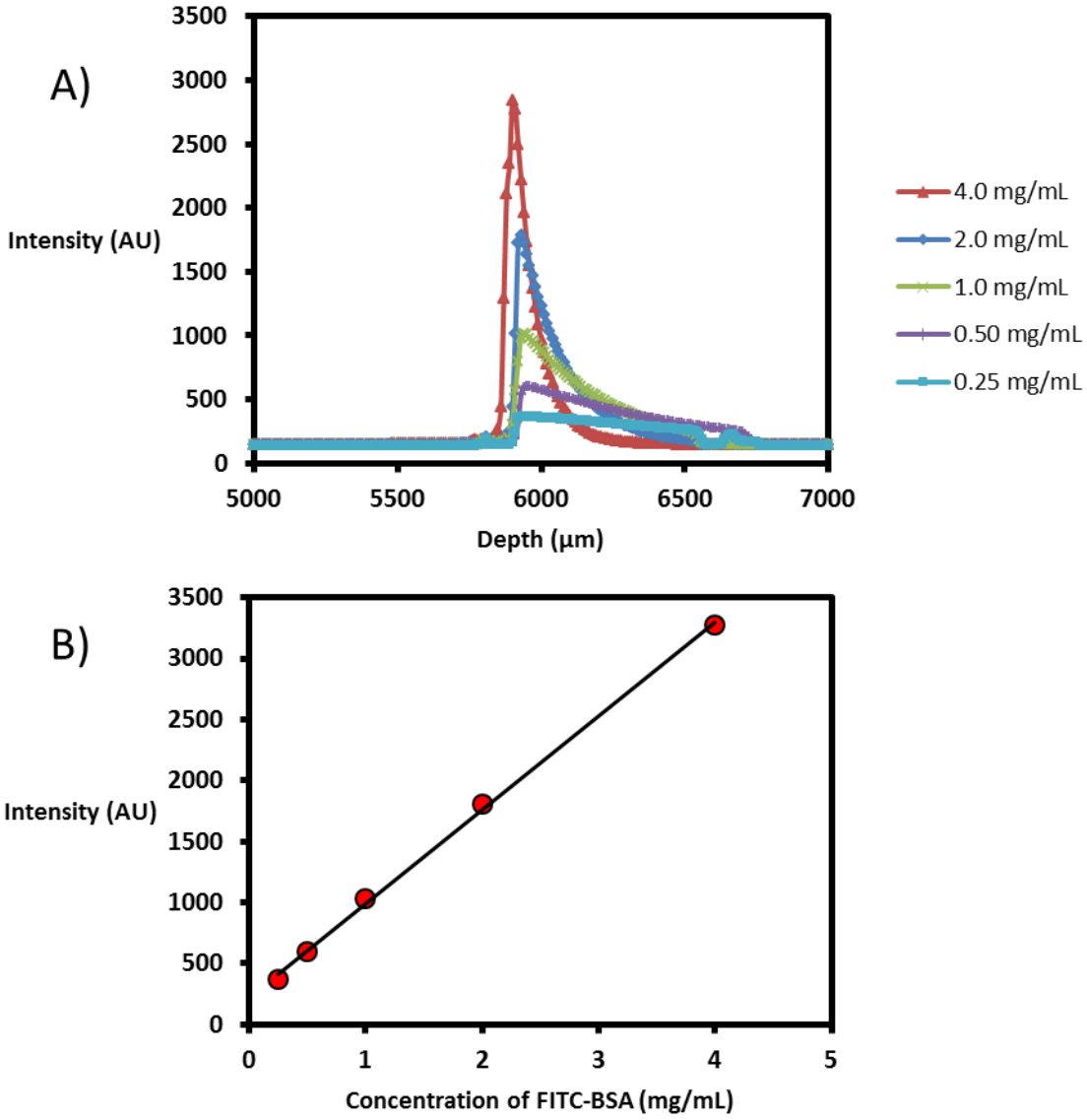

Figure 12: FITC-BSA linear concentration profile

The peaks at 100 µm from the surface of the FRAP slide in A were used to develop the linear profile in B, where the point of maximum intensity represents the surface of the slide. This specific depth was selected to be consistent with the measurement depth used in all FRAP experiments. Each data point is an average of at least three measurements and the error bars are smaller than the markers.

5.3 Physical properties of molecular probes

Fluorescein isothiocyanate-labeled bovine serum albumin (FITC-BSA) and varying dextrans (FDX) were purchased from Sigma Aldrich. To make predictions using the obstruction model, the free diffusion coefficients for the selected probes were obtained from the literature. The hydrodynamic radii of the agents were measured by Watson *et al.*[104] using dynamic light scattering and then estimated, for comparison reasons, by the Stokes-Einstein relationship,

$$r_s = \frac{kT}{6\pi\eta D_0} \qquad [41]$$

where, k is Boltzmann's constant, T is temperature, η is viscosity, r_s is Stokes' radius, and D_0 is the diffusion coefficient at infinite dilution. The physical properties of the agents are described in Table 2.

Table 2. Molecular probe properties

Solute	MW (g/mol)	Sr_s (Å) [a]	HDr_s (Å) [b]	D_0 (μm^2/s)	D_0 ref
FDX-4	4000	13.55	14	161	[105]
FDX-10	10000	17.88	23	122	[105]
FDX-20	20000	29.88	33	74	[106]
FDX-40	40000	46.41	45	47	[105]
FITC-BSA	66700	36.36	36	60	[11]

[a] Stokes' radius. [b] Experimental radius.

5.4 Methacrylation substitution of the modified alginate

The methacrylation substitution of the MALG was determined to be 13% (Figure 13). All the peaks shifted to higher ppm at a temperature of 353 K to separate the overlapping peaks. The substitution was calculated using a ratio of the methylene protons of the methacrylate moieties to the protons of the alginate backbone. The peak at 2.9 ppm represnts residual EDC.[98]

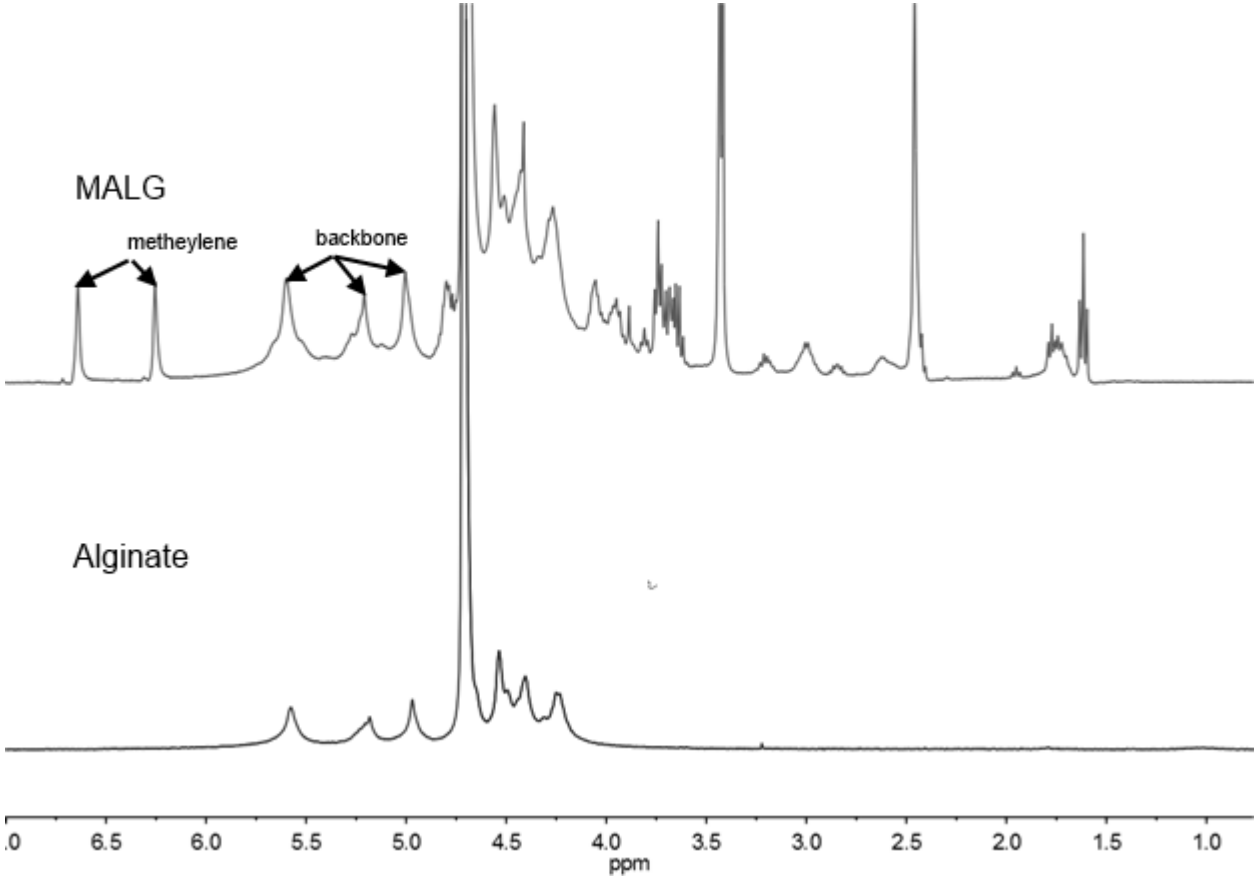

Figure 13: Comparison of the ^{1} H NMR spectra of the native alginate to the MALG

5.5 Validation of the calibrated disk in FRAP

The calibration of the photobleaching disk used in FRAP was investigated using CSLM (Figure 14).

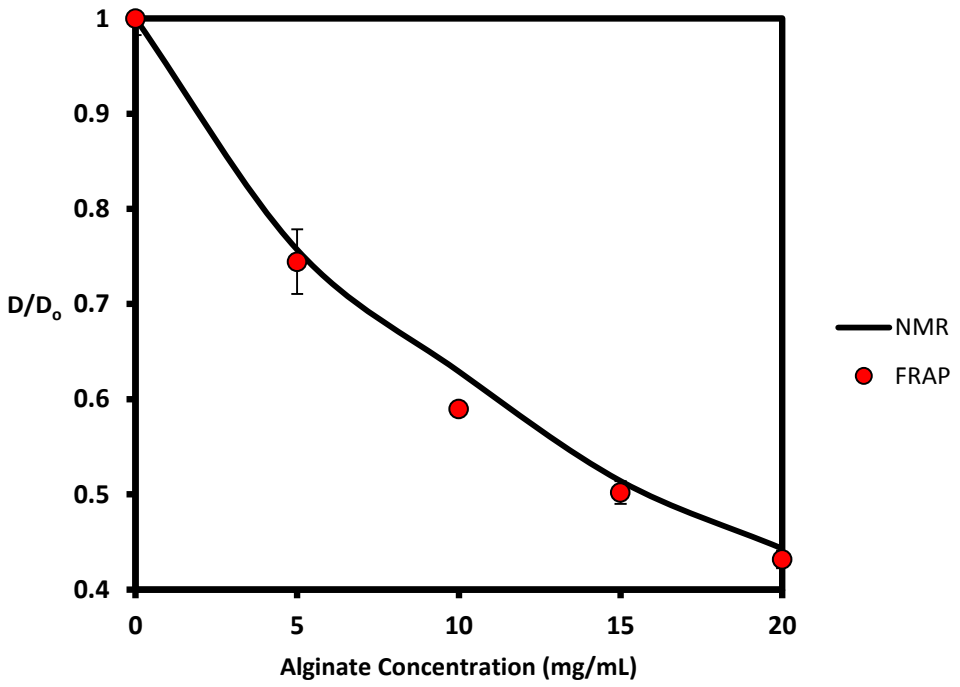

Figure 14: Comparison of the diffusion measurements of FRAP to NMR

The tracer diffusion coefficients of FITC-BSA in sodium alginate solutions obtained by FRAP (red dots) were compared to the diffusion coefficients obtained by Zhang and Amsden using NMR (solid line).[11] Each data point is an average of three measurements and the error bars represent the standard deviation. The size of the disk was first calibrated to the free diffusion coefficient of FITC-BSA (60 $\mu m^2/s$) resulting in a disk diameter of 30 µm, then measurements were taken to verify whether the calibration process was able to provide accurate diffusion coefficients of the alginate solutions.[11] Figure 14 conveys a consistent relationship between the diffusion measurements of FRAP and NMR. It was necessary to calibrate the disk because the diameter of the ROI was determined to have a direct correlation to the extracted diffusion coefficient. In a study by Braeckmans *et al.*, the uniform disk model was developed to provide measurements that were independent of the disk radius.[107] Without an independent ROI, it was impossible

to carry out an experiment using the UDM. A calibration approach was proposed to provide a protocol to define a photobleaching disk within the limitations of the UDM, regardless of its influence on the diffusion coefficient. If such a disk could be defined, then the FRAP model would be applicable to any fluorophore with knowledge of its free diffusion coefficient. The data suggests that the calibration method is appropriate for use with the uniform disk model.

5.6 FRAP measurements with the CSLM in hydrogels

The tracer diffusion coefficients of FITC-dextran (4, 10, 20, and 40 kDa) in alginate-methacrylate hydrogels were measured by FRAP and then compared to the predictions of the obstruction model. The resulting figures have been divided into two different categories: small diffusing probes (Figure 15) and large diffusing probes (Figure 16),

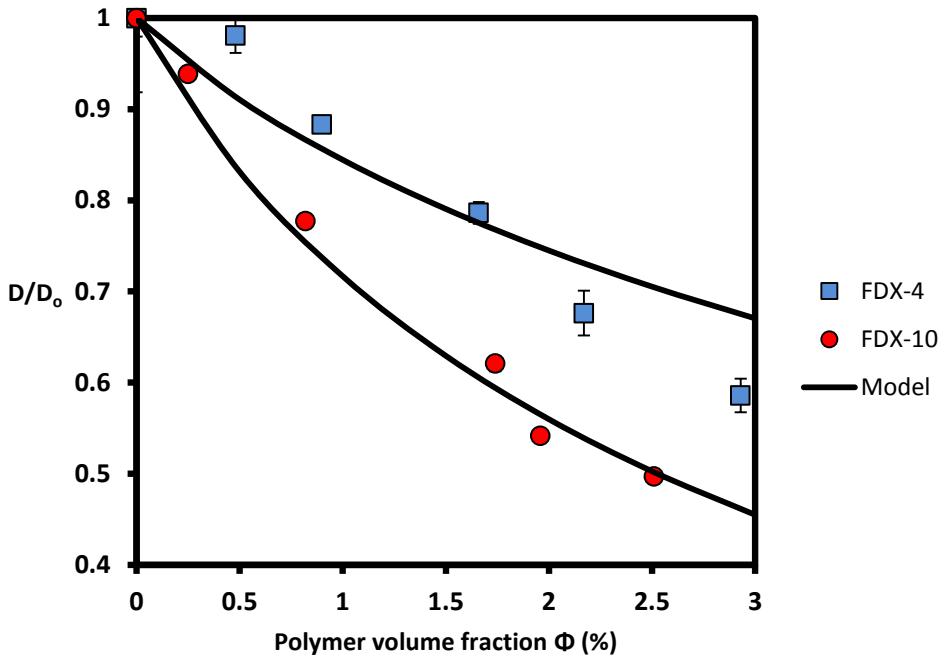

Figure 15: FRAP measurements of FITC-dextrans in hydrogels (small diffusing probes)

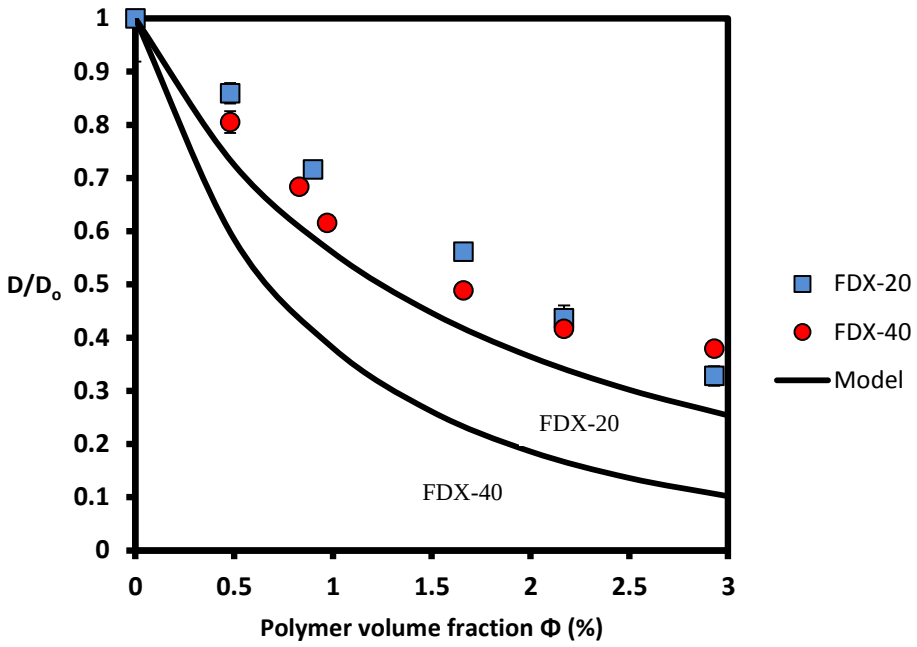

Figure 16: FRAP measurements of FITC-dextrans in hydrogels (large diffusing probes)

Figure 15 conveys a good fit for the obstruction-scaling model to the diffusion profile of the small diffusing probes, FDX-10 and FDX-4. On the other hand, the predicted coefficients in Figure 16 were underestimated by the model for larger probes such as FDX-20 and FDX-40. The obstruction model in both figures utilized the hydrodynamic radii measured by Watson *et al.*. Each data point is an average of three measurements and the error bars represent the standard deviation. The diffusion measurements using FRAP were calibrated to the free diffusion coefficients obtained from the literature for each probe, for which the resulting disk diameters would range from 24-40 μm. It is reasonable to assume that the model's limitations to high molecular weight dextrans stems from their tendency to exhibit reptation. Reptation theory, as it was originally proposed by de Gennes, describes the movement of a polymer chain as a snake-like entity that can weave throughout a network, often resulting in an observed decrease in tortuosity in comparison to other agents such as spheres.[12] For this reason, high molecular weight dextrans are outside the limitations of the obstruction-scaling model, which was derived on the assumption that the diffusant is spherical and non-reptating. Molecular proteins like FITC-BSA and Ovalbumin were initially

selected to be the model probes within this study but these proteins demonstrated strong interactions between the networks of the alginate-methacrylate hydrogels, presumably between the residual methacrylate moieties and the solute. Therefore, proteins in general were inappropriate for measuring tracer diffusion in the methacrylate hydrogels, as neither the UDM nor the obstruction model consider interactions between the network and the probe. FITC-dextran was selected as an alternative diffusant for its well-characterized properties in the literature and strong fluorescence/photobleaching capability.

The diffusion coefficients of varying dextrans (3, 10, 40, and 70 kDa) were compared to the obstruction model using fluorescence correlation spectroscopy in a recent study by Mahmood *et al.*. The obstruction-scaling model demonstrated a poor fit to high molecular weight dextrans as was demonstrated in this study, although they used an older version of the model and, judging from the form, was likely obtained from a review by Masaro *et al.*.[32] The group attributed the limitations of the model to reptation effects, corroborating the results obtained in Figure 16.

A comparison of the generalized model to the solute probes that were tested was plotted in Figure 17,

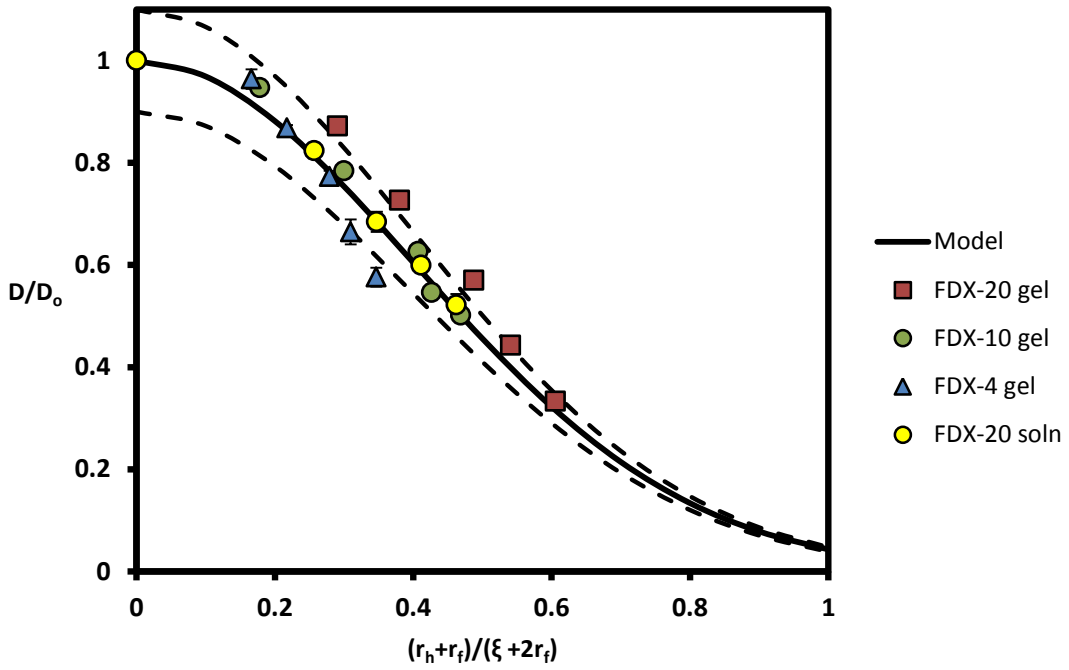

Figure 17: Plot in generic form as reduced diffusion vs $(r_h+r_f)/(\xi+2r_f)$ using experimental r_h values

The data conveys a good fit for the obstruction-scaling model to the diffusion profile of the probes within a 10% range of error (dotted lines). Each data point is the average of at least three measurements and the error bars represent the standard deviation. The obstruction-scaling model demonstrates the ability to predict the spontaneous diffusion coefficients of solute in hydrogels within the constraints of its derived assumptions. By extension, its derived assumptions are suggested to be valid. However, as the solute radius of an agent like dextran approaches the correlation of a hydrogel, it becomes apparent that the obstruction model can no longer provide accurate predictions as a result of high reptation. Otherwise the model conveys a good fit between the observed and the predicted for non-reptating dextran agents.

Chapter 6

Conclusion and recommendations

The tracer diffusion of various dextrans (4, 10, 20, and 40 kDa) through alginate-methacrylate hydrogels has been studied using FRAP. It has been shown that, for dextrans of low molecular weight, the spontaneous diffusion can be successfully described by the obstruction-scaling model, whereas an underestimation of the diffusion was observed for the dextrans of molecular weight above 20 kDa. It was reasonable to assume that this difference was the result of reptation effects. As the radius of a solute approaches the correlation length of a gel, the effects of reptation observed in linear polymers like dextran may reduce the overall tortuosity on the diffusant. The obstruction model does not take these effects into consideration and, therefore, is limited within its predictions. The assumption that the correlation length of a network is the same as that of a solution at equivalent concentration is suggested to be valid in the model's good fit within the limitations of its derived assumptions. The 40 kDa molecular dextran was inconsistent with these assumptions and, as a result, provides little information on the model's validity aside from outlining its limitation to reptating agents. For future work, it is recommended to observe the diffusion of other large neutral diffusants that are spherical and non-reptating, such as dendrimers. These agents would likely need to be characterized and, therefore, it is recommended to carry out a full experiment, including measurements of the solute at infinite dilution using NMR, radius of gyration using MALLS, and solute radius via DLS. It may also be constructive to measure the correlation length of the gels to circumvent the necessity to apply scaling relationships.

References

1. Park, K., Shalaby, W. & Park, H. *Biodegradable Hydrogels for Drug Delivery*. 252 (Technomic Publishing Company, 1993).

2. Amsden, B. Solute Diffusion within Hydrogels. Mechanisms and Models. *Macromolecules* **31,** 8382–8395 (1998).

3. Hoare, T. R. & Kohane, D. S. Hydrogels in drug delivery: Progress and challenges. *Polymer (Guildf).* **49,** 1993–2007 (2008).

4. Ganji, F., Vasheghani-Farahani, S. & Vasheghani-Farahani, E. Theoretical description of hydrogel swelling: a review. *Iran. Polym. J.* **19,** 375–398 (2010).

5. Haraguchi, K. & Takehisa, T. Nanocomposite hydrogels: a unique organic-inorganic network structure with extraordinary mechanical, optical, and swelling/de-swelling properties. *Adv. Mater.* 1120–1124 (2002).

6. Omidian, H., Rocca, J. G. & Park, K. Advances in superporous hydrogels. *J. Control. Release* **102,** 3–12 (2005).

7. Stammen, J. a, Williams, S., Ku, D. N. & Guldberg, R. E. Mechanical properties of a novel PVA hydrogel in shear and unconfined compression. *Biomaterials* **22,** 799–806 (2001).

8. Tan, H., Chu, C. R., Payne, K. a & Marra, K. G. Injectable in situ forming biodegradable chitosan-hyaluronic acid based hydrogels for cartilage tissue engineering. *Biomaterials* **30,** 2499–506 (2009).

9. Rolando Barbucci Ed. *Hydrogels: Biological Properties and Applications*. 212 (Springer-Verlag, 2009).

10. Amsden, B. An Obstruction-Scaling Model for Diffusion in Homogeneous Hydrogels. *Macromolecules* **32,** 874–879 (1999).

11. Zhang, Y. & Amsden, B. G. Application of an Obstruction-Scaling Model To Diffusion of Vitamin B 12 and Proteins in Semidilute Alginate Solutions. *Macromolecules* **39,** 1073–1078 (2006).

12. De Gennes, P. *Scaling Concepts in Polymer Physics*. (Cornell University Press, 1979).

13. Dou, S. & Colby, R. H. Solution Rheology of a Strongly Charged Polyelectrolyte in Good Solvent. *Macromolecules* **41,** 6505–6510 (2008).

14. Weber, L. M., He, J., Bradley, B., Haskins, K. & Anseth, K. S. PEG-based hydrogels as an in vitro encapsulation platform for testing controlled beta-cell microenvironments. *Acta Biomater.* **2,** 1–8 (2006).

15. Brahim, S., Narinesingh, D. & Guiseppi-Elie, A. Polypyrrole-hydrogel composites for the construction of clinically important biosensors. *Biosens. Bioelectron.* **17,** 53–9 (2002).

16. Schägger, H. & von Jagow, G. Tricine-sodium dodecyl sulfate-polyacrylamide gel electrophoresis for the separation of proteins in the range from 1 to 100 kDa. *Anal. Biochem.* **166,** 368–79 (1987).

17. Drury, J. L. & Mooney, D. J. Hydrogels for tissue engineering: scaffold design variables and applications. *Biomaterials* **24,** 4337–4351 (2003).

18. Dong, L. & Hoffman, A. Thermally reversible hydrogels: III. Immobilization of enzymes for feedback reaction control. *J. Control. release* **4,** 223–227 (1986).

19. Hiratani, H. The nature of backbone monomers determines the performance of imprinted soft contact lenses as timolol drug delivery systems. *Biomaterials* **25,** 1105–1113 (2004).

20. Chan, A. W., Whitney, R. a & Neufeld, R. J. Semisynthesis of a controlled stimuli-responsive alginate hydrogel. *Biomacromolecules* **10,** 609–16 (2009).

21. Chan, A. W. & Neufeld, R. J. Tuneable semi-synthetic network alginate for absorptive encapsulation and controlled release of protein therapeutics. *Biomaterials* **31,** 9040–7 (2010).

22. Nakamura, K. *et al.* Oral insulin delivery using P(MAA-g-EG) hydrogels: effects of network morphology on insulin delivery characteristics. *J. Control. release* **95,** 589–99 (2004).

23. Chan, A. W. & Neufeld, R. J. Modeling the controllable pH-responsive swelling and pore size of networked alginate based biomaterials. *Biomaterials* **30,** 6119–29 (2009).

24. Gibas, I. & Janik, H. Review: synthetic polymer hydrogels for biomedical applications. *Chem. Chem. Technol.* **4,** (2010).

25. Xinming, L. *et al.* Polymeric hydrogels for novel contact lens-based ophthalmic drug delivery systems: a review. *Cont. Lens Anterior Eye* **31,** 57–64 (2008).

26. Nicolson, P. C. & Vogt, J. Soft contact lens polymers: an evolution. *Biomaterials* **22,** 3273–83 (2001).

27. Wang, B., Siahaan, T. & Richard, S. *Drug Delivery Principles and Applications*. *Drug Deliv.* 189–192 (John Wiley & Sons, 2005).

28. Gehrke, S. in *Transp. Pharm. Sci.* **11,** 473–546 (Marcel Dekker, 2000).

29. Lobo, V. Mutual diffusion coefficients in aqueous electrolyte solutions. *Pure Appl. Chem.* **65,** 2613–2640 (1993).

30. Fick, A. Ueber Diffusion. *Physics (College. Park. Md).* 59 (1855).

31. Ercken M, Adriaensens P, Vanderzande D, G. J. Study of solvent diffusion in polymeric materials using magnetic-resonance-imaging. *Macromolecules* **25,** 8541 (1995).

32. Masaro, L. & Zhu, X. . Physical models of diffusion for polymer solutions, gels and solids. *Prog. Polym. Sci.* **24,** 731–775 (1999).

33. Weisenberger, L. & Koenig, J. NMR imaging of diffusion processes in polymers: measurement of the spatial dependence of solvent mobility in partially swollen PMMA rods. *Macromolecules* **23,** 2445 (1990).

34. Cuckeir, R. Diffusion of Brownian spheres in semidilute polymer solutions. *Macromolecules* **17,** 252 (1984).

35. Altenberger, A., Tirrell, M. & Dahler, J. Hydrodynamic screening and particle dynamics in porous media, semidilute polymer solutions and polymer gels. *J Chem Phys* **84,** 5122 (1986).

36. Phillies, G. Universal scaling equation for self-diffusion by macromolecules in solution. *Macromolecules* **19,** 2367 (1986).

37. Fujita, H. Diffusion in polymer-diluent systems. *Polym Sci* **3,** 1 (1961).

38. Yasuda, H., Lamaze, C. & Ikenberry, L. Permeability of solutes through hydrated polymer membranes. Part I. Diffusion of sodium chloride. *Die Makromol. Chemie* **118,** 19 (1968).

39. Huglin, M. *Hydrogels in medicine and pharmacy, Vol 1: fundamentals*. 57 (CRC Press, 1986).

40. Fricke, H. A Mathematical Treatment of the Electric Conductivity and Capacity of Disperse Systems I. The Electric Conductivity of a Suspension of Homogeneous Spheroids. *Phys. Rev.* **24,** 575 (1924).

41. Ogston, G., Preston, B. & Wells, J. On the transport of compact particles through solutions of chain-particles. *Proc. R. Soc. Lond.* **333,** 297 (1973).

42. Mackie, J. & Meares, P. The diffusion of electrolytes in a cation-exchange resin membrane. II. Experimental. *Proc. R. Soc. Lond.* **232,** 498 (1955).

43. Amsden, B. Modeling solute diffusion in aqueous polymer solutions. *Polymer (Guildf).* **43,** 1623–1630 (2002).

44. Schaefer, D. A unified model for the structure of polymers in semidilute solution. *Polymer (Guildf).* **2,** 387–394 (1984).

45. Teraoka, I. *Polymer Solutions: An Introduction to Physical Properties*. (John Wiley & Sons, 2002).

46. Ogston, G. The spaces in a uniform random suspension of fibres. *Trans. Faraday Soc* **54,** 1754 (1958).

47. Westrin, B. A., Axelssonb, A. & Zacchib, G. Diffusion measurement in gels. **30,** 189–199 (1994).

48. Lamberti, G., Cascone, S., Titomanlio, G. & Barba, A. . Controlled Release of Drugs From Hydrogel Based Matrices Systems: Experiments and Modeling. *Chem. Biochem. Eng. Q.* **26,** 321–330 (2012).

49. Amsden, B. & Turner, N. Diffusion Characteristics of Calcium Alginate Gels. *Biotechnol. Bioeng.* **65,** 605–10 (1999).

50. Higuchi, T. Rate of release of medicaments from ointment bases containing drugs in suspensions. *J. Pharm. Sci.* **52,** 874–875 (1961).

51. Korsmeyer, R., Gurny, R., Doelker, E., Buri, P. & Peppas, N. Mechanisms of solute release from porous hydrophilic polymers. *Int. J. Pharm* **15,** 25–35 (1983).

52. Johnson, C. Diffusion ordered nuclear magnetic resonance spectroscopy: principles and applications. *Prog. Nucl. Magn. Reson. Spectrosc.* **34,** 203–256 (1999).

53. Braeckmans, K., Peeters, L., Sanders, N. N., De Smedt, S. C. & Demeester, J. Three-dimensional fluorescence recovery after photobleaching with the confocal scanning laser microscope. *Biophys. J.* **85,** 2240–52 (2003).

54. Vikstrom, K. L., Lim, S. S., Goldman, R. D. & Borisy, G. G. Steady state dynamics of intermediate filament networks. *J. Cell Biol.* **118,** 121–9 (1992).

55. Peeters, L. *et al.* Vitreous: a barrier to nonviral ocular gene therapy. *Invest. Ophthalmol. Vis. Sci.* **46,** 3553–61 (2005).

56. Smisdom, N. *et al.* Fluorescence recovery after photobleaching on the confocal laser-scanning microscope: generalized model without restriction on the size of the photobleached disk. *J. Biomed. Opt.* **16,** 046021 (2011).

57. Abbaci, M., Barberi-Heyob, M., Blondel, W., Guillemin, F. & Didelon, J. Advantages and limitations of commonly used methods to assay the molecular permeability of gap junctional intercellular communication. *Biotechniques* **45,** 33–52, 56–62 (2008).

58. Braeckmans, K. *et al.* Line FRAP with the confocal laser scanning microscope for diffusion measurements in small regions of 3-D samples. *Biophys. J.* **92,** 2172–83 (2007).

59. Mazza, D. *et al.* A new FRAP/FRAPa method for three-dimensional diffusion measurements based on multiphoton excitation microscopy. *Biophys. J.* **95,** 3457–69 (2008).

60. Sprague, B. L. & McNally, J. G. FRAP analysis of binding: proper and fitting. *Trends Cell Biol.* **15,** 84–91 (2005).

61. Hagman, J. Structure Dynamics and Heterogeneity in Soft Materials Determined by FRAP. (2012).

62. Brandl, F. *et al.* Hydrogel-based drug delivery systems: comparison of drug diffusivity and release kinetics. *J. Control. Release* **142,** 221–8 (2010).

63. Gagnon, M.-A. & Lafleur, M. Self-diffusion and mutual diffusion of small molecules in high-set curdlan hydrogels studied by 31P NMR. *J. Phys. Chem. B* **113,** 9084–91 (2009).

64. Ghi, P. Y., Hill, D. J. T. & Whittaker, A. K. PFG-NMR measurements of the self-diffusion coefficients of water in equilibrium poly(HEMA-co-THFMA) hydrogels. *Biomacromolecules* **3,** 554–9 (2002).

65. Ivarsson, M. Synthesis of silica particles for the use as probe in diffusion by FRAP and NMR- diffusometry. (2013).

66. *The Molecular Probes Handbook: A Guide to Fluorescent Probes and Labeling Technologies*. (Life Technologies Corporation, 2010).

67. Cheever, E., Blum, F. D., Foster, K. R., Mackay, R. A. & Al, C. E. T. Self-Diffusion of Water in Ionic and Nonionic Microemulsions. **104,** (1985).

68. Waggoner, R. A., Blum, F. D. & MacElroy, J. M. D. Dependence of the solvent diffusion coefficient on concentration in polymer solutions. *Macromolecules* **26,** 6841–6848 (1993).

69. Laurent, T. & Björk, I. On the interaction between polysaccharides and other macromolecules: II. The transport of globular particles through hyaluronic acid solutions. *Biochim. Biophys. …* **49,** 351–359 (1963).

70. Muhr, A. H. & Blanshard, J. M. V. Diffusion in gels. *Polymer (Guildf).* **23,** 1012–1026 (1982).

71. Johansson, L., Skantze, U. & Loefroth, J. Diffusion and interaction in gels and solutions. 2. Experimental results on the obstruction effect. *Macromolecules* 6019–6023 (1991).

72. Johansson, L., Elvingson, C. & Loefroth, J. Diffusion and interaction in gels and solutions. 3. Theoretical results on the obstruction effect. *Macromolecules* 6024–6029 (1991).

73. Bu, Z. & Russo, P. Diffusion of dextran in aqueous (hydroxypropyl) cellulose. *Macromolecules* 1187–1194 (1994).

74. Cukier, R. Diffusion of Brownian spheres in semidilute polymer solutions. *Macromolecules* 252–255 (1984). at <http://pubs.acs.org/doi/abs/10.1021/ma00132a023>

75. Mel'nichenko, Y., Klepko, V. & Shilov, V. Self-diffusion of water in gelatin gels: 1. Macroscopic measurements by tracer technique. *Polymer (Guildf).* **34,** 1019–1023 (1993).

76. Park, I., Jr, C. J. & Gabriel, D. Probe diffusion in polyacrylamide gels as observed by means of holographic relaxation methods: search for a universal equation. *Macromolecules* **21,** 1548–1553 (1990).

77. Rotstein, N. & Lodge, T. Tracer diffusion of linear polystyrenes in poly (vinyl methyl ether) gels. *Macromolecules* 1316–1325 (1992).

78. Kosar, T. F. & Phillips, R. J. Measurement of protein diffusion in Dextran solutions by holographic interferometry. *AIChE J.* **41,** 701–711 (1995).

79. Gibbs, S. & Jr, C. J. Pulsed field gradient NMR study of probe motion in polyacrylamide gels. *Macromolecules* 6110–6113 (1991).

80. Masaro, L., Ousalem, M., Baille, W. E., Lessard, D. & Zhu, X. X. Self-Diffusion Studies of Water and Poly(ethylene glycol) in Solutions and Gels of Selected Hydrophilic Polymers. *Macromolecules* **32,** 4375–4382 (1999).

81. Modesti, G., Zimmermann, B., Börsch, M., Herrmann, A. & Saalwächter, K. Diffusion in Model Networks as Studied by NMR and Fluorescence Correlation Spectroscopy. *Macromolecules* **42,** 4681–4689 (2009).

82. Phillies, G. Self and tracer diffusion of polymers in solution. *soft Condens. matter* 1–53 (2004).

83. Cohen, M. H. & Turnbull, D. Molecular Transport in Liquids and Glasses. *J. Chem. Phys.* **31,** 1164 (1959).

84. Zhu, X. & Macdonald, P. Pulsed-gradient spin-echo NMR measurements of the diffusion coefficients of ketones in poly (methyl methacrylate). *Macromolecules* 4345–4351 (1992).

85. Xia, J. & Wang, C. H. Holographic grating relaxation studies of probe diffusion in amorphous polymers. *J. Polym. Sci. Part B Polym. Phys.* **33,** 899–908 (1995).

86. Yasuda, H., Lamaze, C. & Ikenberr, L. Permeability of Solutes through Hydrated Polymer Membranes .I. Diffusion of Sodium Chloride. *Macromol. Chem. Phys.* **118,** 19 (1968).

87. Hennink, W. & Talsma, H. Controlled release of proteins from dextran hydrogels. *J. Control. release* **39,** 47–55 (1996).

88. Vrentas, J. S., Duda, J. L. & Ling, H.-C. Free-volume theories for self-diffusion in polymer–solvent systems. I. Conceptual differences in theories. *J. Polym. Sci. Polym. Phys. Ed.* **23,** 275–288 (1985).

89. Vrentas, J. & Duda, J. Free-volume theories for self-diffusion in polymer–solvent systems. II. Predictive capabilities. *J. Polym. Sci. Polym. Phys. Ed.* **23,** 289–304 (1985).

90. Vrentas, J. S., Duda, J. L. & Hou, a.-C. Evaluation of theories for diffusion in polymer–solvent systems. *J. Polym. Sci. Polym. Phys. Ed.* **23,** 2469–2475 (1985).

91. Peppas, N. & Reinhart, C. Solute diffusion in swollen membranes. Part I. A new theory. *J. Memb. Sci.* **15,** 275–287 (1983).

92. Reinhart, C. T. & Peppas, N. a. Solute diffusion in swollen membranes. Part II. Influence of crosslinking on diffusive properties. *J. Memb. Sci.* **18,** 227–239 (1984).

93. Lustig, S. R. & Peppas, N. a. Solute diffusion in swollen membranes. IX. Scaling laws for solute diffusion in gels. *J. Appl. Polym. Sci.* **36,** 735–747 (1988).

94. Gao, P. & Fagerness, P. Diffusion in HPMC gels. I. Determination of drug and water diffusivity by pulsed-field-gradient spin-echo NMR. *Pharm. Res.* (1995).

95. Axelrod, D., Koppel, D. E., Schlessinger, J., Elson, E. & Webb, W. W. Mobility measurement by analysis of fluorescence photobleaching recovery kinetics. *Biophys. J.* **16,** 1055–69 (1976).

96. Blonk, J., Don, A. & Vanaalst, H. Fluorescence photobleaching recovery in the confocal scanning light microscope. *J. Microsc.* **169,** 363–374 (1993).

97. Deschout, H. *et al.* Straightforward FRAP for quantitative diffusion measurements with a laser scanning microscope. *Opt. Express* **18,** 22886–905 (2010).

98. Jeon, O., Bouhadir, K. H., Mansour, J. M. & Alsberg, E. Photocrosslinked alginate hydrogels with tunable biodegradation rates and mechanical properties. *Biomaterials* **30,** 2724–34 (2009).

99. Donati, I. *et al.* Galactose-substituted alginate 2: conformational aspects. *Biomacromolecules* **5,** 186–96 (2004).

100. Gilles, M., Hudson, A. & Jr, C. B. Stability of water-soluble carbodiimides in aqueous solution. *Anal. Biochem.* **248,** 244–248 (1990).

101. Stephen, A., Phillips, G. & Williams, P. *Food Polysaccharides and Their Applications*. 752 (Taylor & Francis, 2006).

102. Wang, Z.-Y., White, J. W., Konno, M., Saito, S. & Nozawa, T. A small-angle x-ray scattering study of alginate solution and its Sol-Gel transition by addition of divalent cations. *Biopolymers* **35,** 227–238 (1995).

103. King, A.H. *Food Hydrocolloids*. 115–88 (1983).

104. Watson, P. M. D. *et al.* Modelling the endothelial blood-CNS barriers : a method for the production of robust in vitro models of the rat blood-brain barrier and blood-spinal cord barrier. *BMC Neurosci.* **14,** 1 (2013).

105. Zhang, Z., Nadezhina, E. & Wilkinson, K. J. Quantifying diffusion in a biofilm of Streptococcus mutans. *Antimicrob. Agents Chemother.* **55,** 1075–81 (2011).

106. Laurent, T. C., Sundelöf, L. O., Wik, K. O. & Wärmegård, B. Diffusion of dextran in concentrated solutions. *Eur. J. Biochem.* **68,** 95–102 (1976).

107. Wang, X. & Ye, K. Three-dimensional differentiation of embryonic stem cells into islet-like insulin-producing clusters. *Tissue Eng. Part A* **15,** 1941–52 (2009).